Biosensors and Bioelectronics 64 (2015) 311–317

Contents lists available at ScienceDirect

Biosensors and Bioelectronics

journal homepage: www.elsevier.com/locate/bios

A plasmon-assisted fluoro-immunoassay using gold nanoparticle-decorated carbon nanotubes for monitoring the influenza virus

Jaewook Lee [a,e], Syed Rahin Ahmed [b,c], Sangjin Oh [c], Jeonghyo Kim [c], Tetsuro Suzuki [d], Kaushik Parmar [e], Simon S. Park [e], Jaebeom Lee [c,*], Enoch Y. Park [a,b,**]

[a] Research Institute of Green Science and Technology, Shizuoka University, 836 Ohya Suruga-ku, Shizuoka 422-8529, Japan
[b] Department of Bioscience, Graduate School of Science and Technology, Shizuoka University, 836 Ohya Suruga-ku, Shizuoka 422-8529, Japan
[c] Department of Nano Fusion and Cogno-Mechatronics Engineering, Pusan National University, Busan 609-735, Republic of Korea
[d] Department of Infectious Diseases, Hamamatsu University School of Medicine, 1-20-1 Higashi-ku, Handa-yama, Hamamatsu 431-3192, Japan
[e] Department of Mechanical and Manufacturing Engineering, University of Calgary, Calgary, Canada, T2N 1N4

ARTICLE INFO

Article history:
Received 1 August 2014
Received in revised form
3 September 2014
Accepted 6 September 2014
Available online 16 September 2014

Keywords:
Plasmon-assisted fluoro-immunoassay
Gold nanoparticle-decorated carbon nanotube
CdTe quantum dot
Influenza virus detection platform
Plasmonic resonance energy transfer

ABSTRACT

A plasmon-assisted fluoro-immunoassay (PAFI) was developed for the detection of the influenza virus by using Au nanoparticle (Au NP)-decorated carbon nanotubes (AuCNTs) that were synthesized using phytochemical composites at room temperature in deionized water. Specific antibodies (Abs) against the influenza virus were conjugated onto the surface of AuCNTs and cadmium telluride quantum dots (QDs), which had a photoluminescence intensity that varied as a function of virus concentration and a detection limit of 0.1 pg/mL for all three types of influenza viruses examined. The clinically isolated influenza viruses (A/Yokohama/110/2009 (H3N2)) were detected in the range of 50–10,000 PFU/mL, with a detection limit of 50 PFU/mL. From a series of proof-of-concept and clinical experiments, the developed PAFI biosensing system provided robust signal production and enhancement, as well as an excellent selectivity and sensitivity for influenza viruses. This nanoparticle-based technique could be potentially developed as an efficient detection platform for the influenza virus.

1. Introduction

Many kinds of nanomaterials have been recently used in the area of nanobiotechnology research. The unique physicochemical properties of nanomaterials have found a significant number of applications in biosensing, imaging, and drug delivery system (Ahmed et al., 2013; Lee et al., 2014; Leung et al., 2012; Li and Mezzenga, 2013; Wang et al., 2013b). In particular, nanobiosensing systems have gained popularity owing to its high sensitivity, selectivity, and rapid response time (Liu et al., 2012; Yin et al., 2013). The detection techniques used in various nanobiosensing applications include magnetophoresis, electrochemical analysis, plasmonic coupling immunoassays, and fluoro-immunoassays (Draz et al., 2012; Kim et al., 2013; Li et al., 2013; Viet et al., 2013; Zhou et al., 2012, 2013). The plasmon-assisted fluoro-immunoassay (PAFI) has been used to analyze specific biomaterials (Ahmed et al., 2014; Li et al., 2012; Nooney et al., 2010; Sharma et al., 2013b). The PAFI is based on the plasmonic resonance energy transfer (PRET) phenomenon, which causes a photoluminescence (PL) enhancement from the interactions between the plasmonic nanomaterials and the semiconductor nanoparticles (Lee et al., 2004, 2005, 2007). Such hybrid structures can be used to detect the interaction between an antibody (Ab) and its antigen, because of their tuned optical properties. Although numerous plasmonic nanomaterials have been introduced (*e.g.*, gold, silver, platinum, and metal NPs), Au NP-decorated carbon nanotubes (AuCNTs) have received considerable attention, owing to their unique properties. Au NPs are able to exhibit surface plasmon resonance (Jana et al., 2001; Lee et al., 2011b). Carbon nanotubes exhibit electroconductivity and harbor many π electrons on their surfaces (Jariwala et al., 2013; Sun et al., 2011). Thus, AuCNTs are expected to show a synergistic effect owing to their roles as biosensing platforms, signal enhancers, and signal transducers (McAndrew and

* Corresponding author.
** Corresponding author at: Shizuoka University, Research Institute of Green Science and Technology, 836 Ohya Suruga-ku, Shizuoka 422-8529, Japan.
E-mail addresses: jaebeom@pusan.ac.kr (J. Lee), acypark@ipc.shizuoka.ac.jp (E.Y. Park).

http://dx.doi.org/10.1016/j.bios.2014.09.021
0956-5663/

Baxendale, 2013; Sharma et al., 2013a; Wang et al., 2013a; Yick et al., 2013).

Combining the above mentioned heterogeneous materials requires sophisticated strategies in order to conserve carbon nanotube (CNT) structures and to bind two materials without the help of organic bridges. One of the well-known processes for preparing AuCNT nanostructures involves reduction with chemical reducing agents such as sodium borohydride or hydrazine (Yu et al., 2014; Zhang et al., 2013). An alternative process involves thiol- or amine-assisted interactions between Au NPs and CNT surfaces (Georgakilas et al., 2007; Li et al., 2011). Attachment of Au NPs onto CNT surfaces has been attempted using the processes of electrodeposition, DNA hybridization, and chemical reaction (Georgakilas et al., 2007; Gobbo et al., 2013; Li et al., 2011; Li and Cooper-White, 2013; Peng et al., 2009). However, these approaches can cause CNT damage and organic/biological electric resistance, which may adversely affect their electrical and mechanical properties (Hirsch, 2002; Holzinger et al., 2001).

In this study, we suggest a novel and easy method for preparing AuCNTs by using phytochemicals. The synthetic reaction was carried out in deionized (DI) water at room temperature *via* sonication and stirring processes, without resorting to external heating or application of high pressure. No electrochemistry equipment was used in the above procedure. AuCNTs were produced as follows. Au ions were first attached onto the surface of CNTs and they were then reduced to Au NPs on the CNT surface. This process was catalyzed using a mixture of gallic acid and isoflavone phytochemicals, two well-known natural antioxidants (Aruoma et al., 1993; Park et al., 2009) that served as mild reducing agents (Lee et al., 2011a). Furthermore, the generated AuCNTs were applied onto the influenza virus detection platform by using a quantum dot (QDs)-assisted PAFI.

In this study, we developed a PAFI-based detection platform for the influenza virus, using antibody-conjugated AuCNTs and CdTe QDs. In all, we tested three types of influenza viruses, *viz.* the Influenza virus A/Beijing/262/95 (H1N1), the Influenza virus/New Caledonia/20/99IvR116 (H1N1), and the clinically isolated Influenza virus A/Yokohama/110/2009 (H3N2). The minimum detection limit for the influenza virus was 0.1 pg/mL. The clinically isolated influenza virus was also monitored in the range 50–10,000 PFU/mL, with a detection limit of 50 PFU/mL. Our virus detection platform would be immensely useful not only for detecting the influenza virus, but also for detecting various other viruses and viral diseases.

2. Material and methods

2.1. Materials and instruments

$HAuCl_4 \cdot 3H_2O$, multi-walled carbon nanotubes (MWCNTs), gallic acid, EDC, NHS, cadmium perchlorate hydrate, and cysteamine were purchased from Sigma-Aldrich (Milwaukee, WI, USA). Aluminum telluride (Al_2Te_3) was obtained from the Cerac Company (Milwaukee, WI, USA). The isoflavone was isolated from commercial soybeans. 3,3′,5,5′-tetramethylbenzidine was purchased from Dojindo (Osaka, Japan). The ECL™ anti-mouse IgG, horseradish peroxidase (HRP)-conjugated whole antibody (Ab) was obtained from GE Healthcare UK, Ltd. (Buckinghamshire, UK). Goat anti-rabbit IgG-HRP was purchased from Santa Cruz Biotechnology, Inc. (Santa Cruz, CA, USA). Anti-Influenza A virus hemagglutinin (HA) Ab Ab66189, which is a mouse monoclonal antibody [B219M] for the influenza A virus HA H1 and positive against influenza virus A/Beijing/262/95 (H1N1), A/New Caledonia/20/99 (H1N1), and A/Taiwan/1/86 (H1N1), was purchased from Abcam Inc. (Cambridge, UK). Anti-neuraminidase (NA) (New Caledonia/20/1999/(H1N1)), a rabbit polyclonal Ab, was obtained from Immune Technology Corp. (New York, NY, USA). Anti-H3 (H3N2) (Ab82454), a mouse monoclonal Ab [InA227] to H3 (H3N2) that recognizes influenza virus A HA H3, was purchased from Abcam Inc. (Cambridge, UK). Influenza virus New Caledonia/20/99IvR116 (H1N1) and A/Beijing/262/95 (H1N1) were purchased from Sino Biological Inc. (Beijing, China) and HyTest Lyd (Turku, Finland), respectively. Influenza virus A/Yokohama/110/2009 (H3N2) was isolated from a clinically isolated sample, which was kindly provided by Dr. C. Kawakami of Yokohama City Institute of Health, Japan and was used to assess the versatility of this assay system.

The absorbance of AuCNTs and the corresponding PL enhancement were measured using a filter-based multimode microplate reader (Infinite® F500, TECAN, Ltd., Männedorf, Switzerland), and the chemical reactions and surface functional groups were monitored by FT-IR spectroscopy (FT-IR 6300, JASCO, Corp. Tokyo, Japan). The morphologies and sizes of the nanostructures were characterized by TEM (JEM-2100F, JEOL, Ltd., Tokyo, Japan). An X-ray powder diffractometer (RINT ULTIMA, Rigaku, Corp., Tokyo, Japan) was used to characterize AuCNT by using CuKa radiation and a Ni filter. The data were collected from 2 theta=0–100° at a scan rate of 0.01° per step and 10 s per point. The AuCNTs and MWCNTs were analyzed by Raman spectroscopy (HR-800, Lab-RAM, HORIBA Ltd., Kyoto, Japan). In order to measure the electroconductivity, AuCNT solution was dropped on the planar interdigitated electrode (planar IDE-Pt/0.25″, Synkera, USA) and dried at room temperature. Then, the current change of the deposited area was monitored by linear sweep voltammetry from −1 V to 1 V (SP-150, BioLogic, France). A plate reader (Model 680, Bio-Rad, Hercules, USA) was used to confirm the presence of Ab-conjugated nanomaterials. The PL image of the hybrid nanostructure was observed using a confocal laser-scanning microscope (LSM 700, Carl Zeiss Microimaging, GmbH, Göttingen, Germany).

2.2. Synthesis of AuCNTs and CdTe QDs

AuCNTs were synthesized at room temperature by using commercially available reagents. Forty milligrams of MWCNT was dispersed in 100 mL of nitric acid and boiled for 5 h to prepare the hydrophilic MWCNTs. Subsequently, 0.01 mmol of $HAuCl_4 \cdot 3H_2O$ and 2 mg of acid-treated MWCNTs were dispersed in 30 mL of DI water by sonication for 30 min. Subsequently, 600 μL of GI solution was added into the MWCNT/Au ion solution, and then stirred vigorously for 1 h. The GI solution was used as a reducing agent and stabilizer, and prepared as follows: 10 mg of isoflavone was dissolved in 10 mL of the 0.01 M gallic acid solution. The cysteamine-coated CdTe QDs were synthesized as reported in detail elsewhere (Gaponik et al., 2002; Lee et al., 2010).

2.3. Preparation of antibody-conjugated AuCNTs and CdTe QDs

In order to conjugate the Abs to the AuCNTs, amine-functionalized AuCNTs and Ab-conjugated EDC/NHS were prepared. To modify the surface of the Au NPs, 1 mg of AuCNTs was dispersed in 10 mL of DI water. Then, 1 mL of 0.01 M cysteamine was added into the AuCNT solution. After 30 min of stirring, this mixture was centrifuged to separate the amine-functionalized AuCNTs. Additionally, 100 μL of the 4 mM EDC and 10 mM NHS were added in the 96-well plate and incubated and gently shaken for 30 min at 200 rpm with 1 μL of anti-HA Ab (Ab66189) (final concentration of 5 ng/mL) for the EDC/NHS coupling reaction. Finally, 30 μL of the amine-functionalized AuCNT (1 μg/μL) and activated anti-HA Ab (Ab66189) were mixed in all wells and shaken for 3 h for effective bioconjugation. Anti-NA (New Caledonia/20/1999/(H1N1)) and anti-HA (Ab82454) Abs were also conjugated to the surfaces of the Au CNTs by using the same procedure. Anti-HA (Ab66189) and

anti-HA (Ab82454)-conjugated CdTe QDs were also prepared by using the procedure for Ab-conjugated AuCNTs.

2.4. Plasmon assisted fluoro-immunoassay (PAFI) for influenza virus detection

In order to detect the influenza virus *via* PAFI, 45 μL of Ab-conjugated AuCNTs and 45 μL of the CdTe QDs were mixed in each of the 96 wells. Consequently, serially diluted influenza virus was added into each well and shaken for 1 h. During this process, the Ab-conjugated AuCNTs and the CdTe QDs were found to bind each other in the presence of the influenza virus, owing to the affinity between the antigen on the surface of virus and its corresponding antibody. To evaluate the efficacy of PAFI as a detection platform, the following three types of influenza viruses were used: A/Beijing/262/95 (H1N1), New Caledonia/20/99IvR116 (H1N1), and A/Yokohama/110/2009 (H3N2). The PL intensities were measured as a function of the concentration of the influenza virus. The PAFI was carried out at an excitation wavelength of 380 nm, and the excitation and the emission slits were 5 and 10 nm in width, respectively. The PL intensity of this system was monitored at 518 nm during signal detection. In order to evaluate the PAFI system with different influenza virus, all detection experiment was carried out over 3 times.

3. Results and discussion

3.1. Design and preparation of AuCNTs for PAFI

The synthesis of AuCNTs comprised two steps (Fig. 1), *viz.* the preparation of plasmonic nanomaterials (step I), and the processing of PAFI for influenza virus detection by using AuCNTs and QDs (step II). Firstly, the acid-treated multi-walled CNTs (MWCNTs) were dispersed in DI water containing a gold precursor (Au^{3+}) by using sonication. Owing to the π-electrons and oxygen moieties on the surface of the acid-treated MWCNTs, Au^{3+} is able to attach onto the surface of MWCNTs through electrostatic attraction. In order to decorate Au NPs onto the MWCNTs, the Au ions were reduced to Au NPs, using a mixture of gallic acid and isoflavone (GI solution). AuCNTs were obtained after 1 h of stirring and washing with DI water. To perform the PAFI for influenza virus detection by using AuCNTs, anti-hemagglutinin (HA) Ab or anti-neuraminidase (NA) Ab specific for the influenza virus were conjugated onto the surfaces of AuCNTs and QDs by using a *N*-ethyl-*N*′-(dimethylaminopropyl) carbodiimide (EDC)/*N*-hydroxysuccinimide (NHS)-coupling reaction (step II in Fig. 1). In the presence of the influenza virus, the distance between the Ab-conjugated AuCNTs and the QDs diminishes by an affinity between an antigen and its Ab. Depending on the concentration of the influenza virus, the formation of the AuCNT and QD hybrid structures caused a variation in the PL intensities. In the PAFI system, plasmonic material is not single Au NP but AuCNT assembly structure. Thus the energy transfer to enhance the PL property would be taken a place at the sandwich structure between plasmonic AuCNT structure and fluorescent CdTe QDs with virus. Moreover, this sandwich structure could lead the PL enhancement through the collective effect between plasmonic materials and fluorescent nanoparticles (Lee et al., 2004).

3.2. Morphology of AuCNTs

In order to confirm the decoration of Au NPs onto MWCNTs, the morphology of MWCNTs and AuCNTs were examined using transmission electron microscopy (TEM). The MWCNTs showed the presence of a slick surface that was over 3 μm in length (Figs. 2A and S1A, respectively). However, after two steps of the decoration reaction, a large number of Au NPs were detected on the surface of MWCNTs (Figs. 2B and S1B). The carbon structure of MWCNT is transparent, but as heavy metals show high electron absorption, Au NPs are easily distinguishable in the TEM images. The average particle size of the Au NPs was 20 nm, and they were

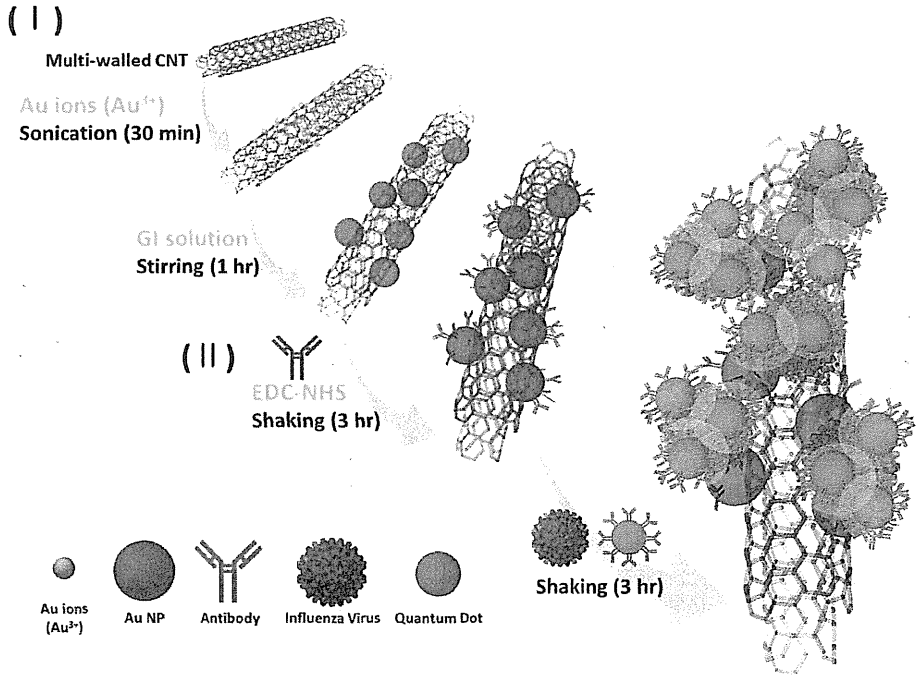

Fig. 1. (I) Synthetic scheme for the preparation of Au nanoparticle (NP)-decorated CNT nanostructures (AuCNTs) and (II) the process of influenza virus detection by using PAFI, non-scalable.

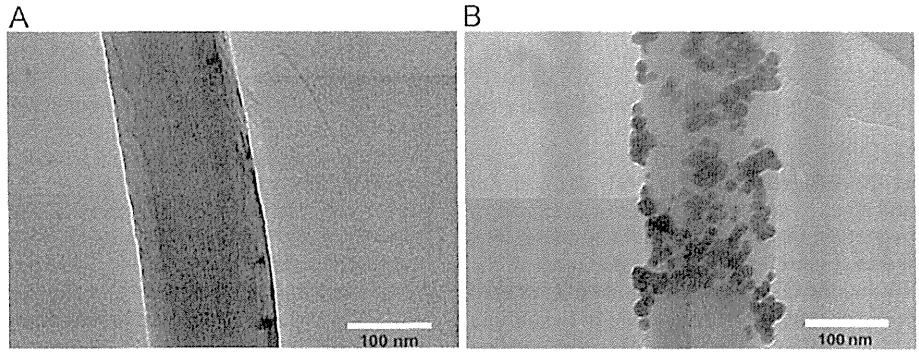

Fig. 2. TEM images of (A) MWCNTs and (B) AuCNTs.

well dispersed with a high density over the large surface area of the MWCNTs (Fig. S1B).

3.3. *Optical, surface-enhanced Raman scattering, physicochemical, and electrical properties of AuCNTs*

The optical absorbance of AuCNTs was measured using a filter-based absorbance-mode microplate reader. Typically, the plasmon peak of Au NPs that are 20 nm in radius occurs at 525 nm. However, the surface plasmonic absorbance of Au NPs was observed as a black spectrum at 550 nm (Fig. 3A), and its bands were broadened and non-symmetric; however, large-sized (> 50 nm) particles were not observed in the corresponding TEM image. Plasmon-coupling between adjacent Au NPs might have occurred, owing to the delocalized π-electron cloud on the surface of MWCNTs. This interaction caused a broadened and non-symmetric plasmonic band of Au NPs. Thus MWCNT can play a role as mediator for plasmonic coupling interaction, thus optical property of this hybrid structure could be enhanced (Lee et al., 2012). However, in the MWCNT case, the specific absorbance as plasmonic peak was not observed by UV/vis spectroscopy. Thus, only MWCNT was not suitable for PAFI detection platform. The structural characteristics of the AuCNTs were elucidated based on the powder X-ray diffraction (XRD) pattern (Fig. 3B). A strong diffraction peak corresponding to the 002 plane of the MWCNTs was presented at 2 theta=26.2° in the XRD pattern (ICSD card no: 01-075-1621). Meanwhile, several new diffraction patterns and weak carbon peaks were measured in the AuCNTs (Fig. 3B, red pattern). The presence of Au NPs in the nanostructure was confirmed by the characteristic diffraction peaks from the face-centered cubic packing arrangement of bulk Au *i.e.*, the (111), (200), (220), (311), (222), and (400) planes at 2 theta values of 38.2°, 44.4°, 64.6°, 77.5°, 81.7°, and 98.1° (ICSD card no: 00-004-0784), respectively. Au NPs possess a higher crystallinity than the carbon structures, because of the metal NPs. Thus, the diffraction patterns of Au NPs were stronger than those of the carbon face. The surface-enhanced Raman scattering (SERS) was measured by Raman spectroscopy at the excitation wavelength of 514 nm (Fig. 3C). The peak at 1340 cm^{-1} indicates that the D band occurred due to the local disorder present in the AuCNT structure

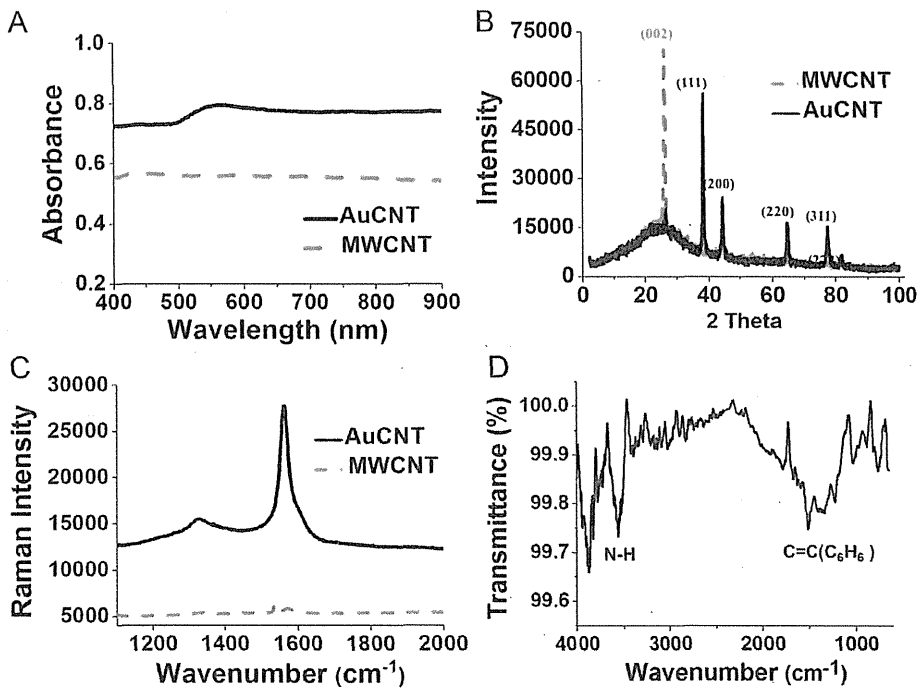

Fig. 3. Physicochemical properties of the AuCNTs. (A) UV/vis spectra, (B) XRD data, (C) Raman spectra of MWCNT with Au ions (red dash line) and AuCNTs (black line), and (D) FT-IR spectra of the amine-functionalized AuCNTs. (For interpretation of the references to color in this figure legend, the reader is referred to the web version of this article.)

(Sharma et al., 2013a). In addition, a G peak appeared near 1580 cm^{-1}, which is related to the characteristic feature (especially to the sp^2-hybridized carbon allotropes) of the graphitic layers (Baro et al., 2013). As expected, the Raman spectrum intensity was more enhanced in the AuCNTs than in the MWCNTs (Sharma et al., 2013a) The spectrum intensity of AuCNTs was 5 times higher than that of MWCNTs. Therefore, the SERS effect was induced by decoration of Au NPs onto the MWCNT surface. The functional group of the amine-functionalized AuCNT was analyzed using Fourier Transform Infrared (FT-IR) spectroscopy. For the EDC/NHS coupling reaction with the carboxylic group of the influenza virus antibody, the N-H vibration of AuCNT was detected around 1250 cm^{-1} and 3400–3500 cm^{-1} (Fig. 3D), respectively. These bands around 1450–1580 cm^{-1} are characteristic of the aromatic bonds of MWCNT. The C–O single-bond vibration was observed at 1010 cm^{-1}. The electroconductivities of the AuCNTs and MWCNTs were measured using a finger type Pt electrode *via* the linear sweep method. The average linear resistance of AuCNT was approximately 0.007 mΩ, whereas that of MWCNT was much higher (Fig. S2). From these physicochemical results, it was evident that the AuCNT composite exhibits enhanced properties such as SERS and electrical conductivity. Furthermore, we could experimentally establish the fact that critical damage to the AuCNT structure indeed did not occur, and that AuNPs were directly attached onto the surface of the CNTs, owing to a mild reduction reaction.

3.4. *PAFI performance for influenza virus detection by using AuCNT*

In order to assess the PAFI performance for the influenza virus detection, three types of antibodies, *viz.* anti-HA (H1) (Ab66189), anti-neuraminidase (NA) (New Caledonia/20/1999/(H1N1)), and anti-HA (H3N2) (Ab82454) were conjugated onto the surface of AuCNTs (step II in Fig. 1). In addition, the surfaces of CdTe QDs were also conjugated with anti-HA (H1) (Ab66189) and anti-HA (H3N2) (Ab82454) antibodies by using the same method. In this case, the Ab-conjugated AuCNTs play the role of plasmon-supplying substrates, whereas the Ab-conjugated CdTe QDs act as PL-monitoring materials. Prior to virus detection, conjugation of the Abs to the AuCNTs or CdTe QDs was verified using an ELISA (Fig. S3). Anti-HA (Ab66189) and anti-NA (New Caledonia/20/1999/ (H1N1))-conjugated AuCNTs, and anti-HA (Ab66189)-conjugated CdTe QDs displayed strong signals (Fig. S3A, B, and C, respectively). In the case of the anti-HA (Ab82454)-conjugated AuCNTs and the CdTe QDs, the recorded absorbance was lower than that of the other Ab-conjugated NPs (Fig. S4). These results indicate that all antibodies were successfully conjugated onto the surface of the AuCNTs and the CdTe NPs.

The Ab-conjugated nanostructures were used for constructing the PAFI system. The detection of the influenza virus was made possible by using a confocal laser-scanning microscope (Fig. 4). Influenza virus A/Beijing/262/95 (H1N1) was dosed into the anti-HA Ab-conjugated AuCNTs and onto the CdTe system. In the presence of the virus, the distance between the HA Ab-conjugated AuCNTs and the HA Ab-conjugated CdTe QDs was reduced, owing to the affinity between the antigen on the surface of the virus and conjugated antibody. Subsequently, the hybrid nanowire structure showed green PL (Fig. 4D–F). However, no PL was observed at all in the absence of the virus (Fig. 4A–C).

In addition, the sensitivity of the PAFI was demonstrated with two different influenza viruses; A/Beijing/262/95 (H1N1) and New Caledonia/20/99IvR116 (H1N1), respectively. All procedures were

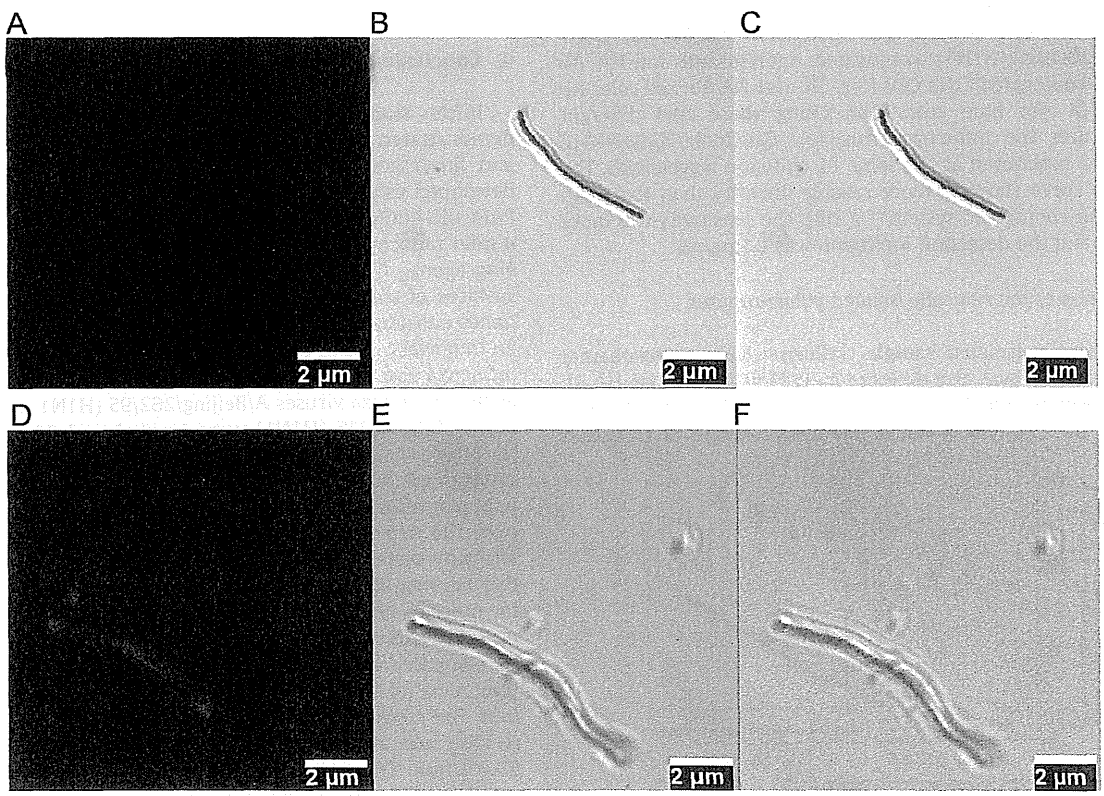

Fig. 4. Confocal laser-scanning microscopy images of the AuCNT-QD hybrid structure obtained *via* the anti-HA Ab conjugation reaction with influenza virus A/Beijing/262/95 (H1N1). (A)–(C) Before and (D)–(F) after the conjugation reaction with influenza virus. (A) and (D) are fluorescent images; (B) and (E) are DIC images; (C) and (F) are merged images.

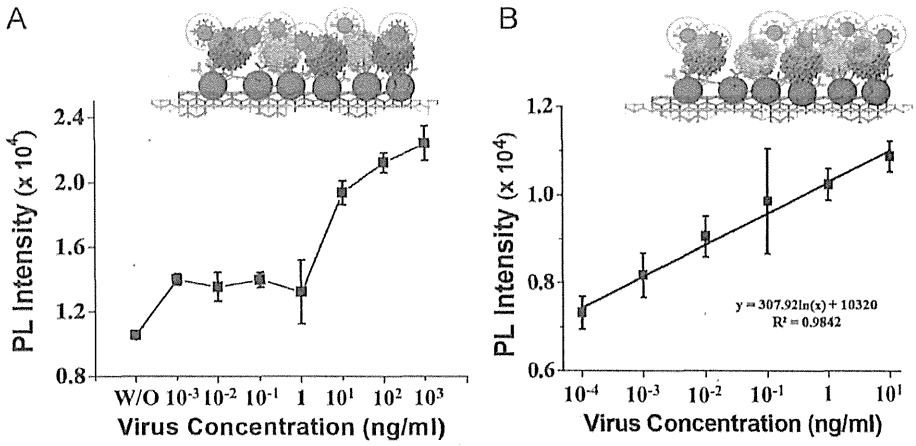

Fig. 5. The calibration curve of the PL intensity corresponding to the concentration of (A) Influenza virus A/Beijing/262/95 (H1N1) and (B) Influenza virus/New Caledonia/20/99IvR116 (H1N1). (For interpretation of the references to color in this figure, the reader is referred to the web version of this article.)

carried out in a 96-well plate. As the concentration of the influenza virus was increased, the PL intensity corresponding to both of the viruses also increased (Fig. S5). This implies that the binding affinity between the Ab-conjugated AuCNTs and the CdTe QDs was dependent on the virus concentration. Furthermore, using anti-HA Ab (Ab66189)-conjugated AuCNTs and CdTe QDs, we carried out the PAFI for the influenza virus A/Beijing/262/95 (H1N1). The detection was carried out at 518 nm, and a calibration curve corresponding to the virus concentrations was obtained (Fig. 5A). In this case, the detection limit was 1 ng/mL. As the same antibody was conjugated onto the surface of both the nanomaterials, a binding competition took place between the Ab-conjugated AuCNTs and the CdTe QDs against virus. To improve the detection limit of PAFI, various different antibodies were conjugated onto the surface of each of the nanomaterials: anti-NA Ab (New Caledonia/20/1999/(H1N1))-conjugated AuCNTs and anti-HA Ab (Ab66189)-conjugated CdTe QDs (Fig. 5B, anti-NA Ab; red color Ab and anti-HA Ab; blue color Ab). Using these two different nanostructures the influenza virus/New Caledonia/20/99IvR116 (H1N1) was monitored at the same PL emission wavelength. The calibration curve shows a more reliable linearity than that with the same Ab-conjugated system (Fig. 5B). The sensitivity was more improved, and the detection limitation was 0.1 pg/mL.

3.5. Detection of the clinically isolated influenza virus

The clinically isolated sample (influenza virus A/Yokohama/110/2009 (H3N2)) was also detected by PAFI using the anti-HA Ab (Ab82454)-conjugated AuCNTs and CdTe QDs at 518 nm in the 96-well plate. The PL intensity was dramatically changed as a function of the virus concentration. In the presence of the influenza virus, the PL intensity showed an 8-fold increase, as compared to the corresponding intensity in the absence of the same virus (Fig. S6). The calibration curve was obtained in the range 50–10,000 PFU/mL (Fig. 6) and the detection limit was 50 PFU/mL. This implies that the clinically isolated virus was successfully detected by PAFI using the Ab-conjugated AuCNTs and the CdTe QDs. The selectivity of PAFI was confirmed using the anti-HA Ab (Ab66189)-conjugated AuCNTs and the CdTe QDs. The anti-HA Ab (Ab66189) could only recognize the HA present in the influenza virus (H1N1). The PL for influenza virus A/Yokohama/110/2009 (H3N2) was low, similar to that of the negative control (BSA) (Fig. S7).

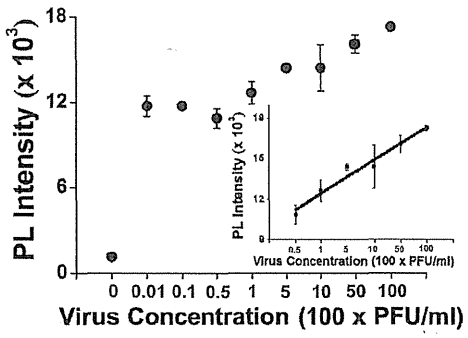

Fig. 6. The calibration curve of the clinically isolated influenza virus A/Yokohama/110/2009 (H3N2).

4. Conclusion

In this study, the influenza virus monitoring was successfully demonstrated by interaction between plasmonic nanomaterials and fluorescent particles. In particular, novel PAFI system was developed using AuCNT and CdTe nanomaterials. To perform the PAFI, the AuCNTs were prepared by a simple 2 step-process, using a mild reducing agent without thermal assistance or harsh reducing agents. A large number of Au NPs were decorated onto the surfaces of the CNTs, and they showed a surface plasmon resonance effect at the AuCNT surface. Thus, the AuCNT surface played an important role as the plasmonic substrate for the PAFI. Various influenza viruses were monitored and the detection limits of PAFI against influenza viruses A/Beijing/262/95 (H1N1) and New Caledonia/20/99IvR116 (H1N1) were 1 ng/mL and 0.1 pg/mL, respectively. For the detection of the New Caledonia virus, two different types of antibodies were attached onto the surface of each of the nanomaterials, and then used for monitoring the virus. In this case, the detection limitation was higher than that of the single antibody system (Beijing virus detection), owing to less competitive binding affinity. In previous reports, the detection limitation for proteins and viruses was reported to be approximately in the ng range (Ahmed et al., 2014; Li et al., 2012; Nooney et al., 2010). As compared to the other PAFI detection systems, the detection limitation for this particular system was improved by about 10-fold. The clinically isolated influenza virus A/Yokohama/110/2009 (H3N2) was also tested, and the corresponding sensitivity was 50 PFU/mL. The PAFI system also showed excellent selectivity, which was 100-fold higher than that of the commercial diagnostic kit. This system may be applied not only to the influenza virus, but also to various other infectious viruses.

Acknowledgment

We wish to thank Dr. C. Kawakami of the Yokohama City Institute of Health, Japan for providing the influenza virus A/Yokohama/110/2009 (H3N2). This work was supported partly by the Promotion of Nanobio-technology Research to support Aging and Welfare Society from the Ministry of Education, Culture, Sports, Science and Technology, Japan. This study was supported by a grant from the Korean Health Technology R&D Project, Ministry of Health & Welfare, Republic of Korea (HI13C0862); and by the Basic Science Research Program through the National Research Foundation of Korea (NRF), funded by the Ministry of Education, Science and Technology (2013004637).

Appendix A. Supplementary information

Supplementary data associated with this article can be found in the online version at http://dx.doi.org/10.1016/j.bios.2014.09.021.

References

Ahmed, S.R., Dong, J.H., Yui, M., Kato, T., Lee, J., Park, E.Y., 2013. J. Nanobiotechnol. 11, 28.
Ahmed, R.S., Hossain, M.A., Youn Park, J., Kim, S.H., Lee, D., Suzuki, T., Lee, J., Park, E. Y., 2014. Biosens. Bioelectron. 58, 33–39.
Aruoma, O.I., Murcia, A., Butler, J., Halliwell, B., 1993. J. Agric Food Chem. 41, 1880–1885.
Baro, M., Nayak, P., Baby, T.T., Ramaprabhu, S., 2013. J. Mater. Chem. A 1, 482–486.
Draz, M.S., Fang, B.A., Li, L.J., Chen, Z., Wang, Y.J., Xu, Y.H., Yang, J., Killeen, K., Chen, F. F., 2012. ACS Nano 6, 7634–7643.
Gaponik, N., Talapin, D.V., Rogach, A.L., Hoppe, K., Shevchenko, E.V., Kornowski, A., Eychmuller, A., Weller, H., 2002. J. Phys. Chem. B 106, 7177–7185.
Georgakilas, V., Gournis, D., Tzitzios, V., Pasquato, L., Guldi, D.M., Prato, M., 2007. J. Mater. Chem. 17, 2679–2694.
Gobbo, P., Biesinger, M.C., Workentin, M.S., 2013. Chem. Commun. 49, 2831–2833.
Hirsch, A., 2002. Angew. Chem. Int. Ed. 41, 1853–1859.
Holzinger, M., Vostrowsky, O., Hirsch, A., Hennrich, F., Kappes, M., Weiss, R., Jellen, F., 2001. Angew. Chem. Int. Ed. 40, 4002.
Jana, N.R., Gearheart, L., Murphy, C.J., 2001. Langmuir 17, 6782–6786.
Jariwala, D., Sangwan, V.K., Lauhon, L.J., Marks, T.J., Hersam, M.C., 2013. Chem. Soc. Rev. 42, 2824–2860.
Kim, J., Lee, J., Lee, K.I., Park, T.J., Kim, H.J., Lee, J., 2013. Sens. Actuators B: Chem. 177, 327–333.
Lee, J., Govorov, A.O., Dulka, J., Kotov, N.A., 2004. Nano Lett. 4, 2323–2330.
Lee, J., Govorov, A.O., Kotov, N.A., 2005. Angew. Chem. Int. Ed. 44, 7439–7442.
Lee, J., Hernandez, P., Lee, J., Govorov, A.O., Kotov, N.A., 2007. Nat. Mater. 6, 291–295.
Lee, J., Kim, H.Y., Zhou, H., Hwang, S., Koh, K., Han, D.W., Lee, J., 2011a. J. Mater. Chem. 21, 13316–13326.
Lee, J., Orazbayev, A., Govorov, A.O., Kotov, N.A., 2010. J. Phys. Chem. C 114, 1404–1410.
Lee, J., Park, E., Lee, J., 2014. Bioprocess Biosyst. Eng. 37, 983–989.
Lee, J., Zhou, H., Lee, J., 2011b. J. Mater. Chem. 21, 16935–16942.
Lee, Y.H., Polavarapu, L., Gao, N., Yuan, P., Xu, Q.H., 2012. Langmuir 28, 321–326.
Leung, K.C.F., Xuan, S.H., Zhu, X.M., Wang, D.W., Chak, C.P., Lee, S.F., Ho, W.K.W., Chung, B.C.T., 2012. Chem. Soc. Rev. 41, 1911–1928.
Li, C.X., Mezzenga, R., 2013. Nanoscale 5, 6207–6218.
Li, H., Chen, C.Y., Wei, X., Qiang, W.B., Li, Z.H., Cheng, Q., Xu, D.K., 2012. Anal. Chem. 84, 8656–8662.
Li, H.Q., Cooper-White, J.J., 2013. Nanoscale 5, 2915–2920.
Li, X.L., Qin, Y.J., Picraux, S.T., Guo, Z.X., 2011. J. Mater. Chem. 21, 7527–7547.
Li, Y.X., Hong, M., Qiu, B., Lin, Z.Y., Cai, Z.W., Chenb, Y.T., Chen, G.N., 2013. Chem. Commun. 49, 10563–10565.
Liu, Y.X., Dong, X.C., Chen, P., 2012. Chem. Soc. Rev. 41, 2283–2307.
McAndrew, C.F., Baxendale, M., 2013. Nanotechnology 24, 305202.
Nooney, R., Clifford, A., LeGuevel, X., Stranik, O., McDonagh, C., MacCraith, B.D., 2010. Anal. Bioanal. Chem. 396, 1127–1134.
Park, J.H., Choi, T.B., Kim, S.W., Hur, M.G., Yang, S.D., Yu, K.H., 2009. Radiat. Phys. Chem. 78, 623–625.
Peng, X.H., Chen, J.Y., Misewich, J.A., Wong, S.S., 2009. Chem. Soc. Rev. 38, 1076–1098.
Sharma, H., Agarwal, D.C., Shukla, A.K., Avasthi, D.K., Vankar, V.D., 2013a. J. Raman Spectrosc. 44, 12–20.
Sharma, P., Kukkar, M., Ganguli, A.K., Bhasina, A., Suri, C.R., 2013b. Analyst 138, 4312–4320.
Sun, F., Cha, H.R., Bae, K., Hong, S., Kim, J.M., Kim, S.H., Lee, J., Lee, D., 2011. Mater. Sci. Eng. A: Struct. Mater. Prop. Microstruct. Process. 528, 6636–6641.
Viet, N.X., Chikae, M., Ukita, Y., Maehashi, K., Matsumoto, K., Tamiya, E., Viet, P.H., Takamura, Y., 2013. Biosens. Bioelectron. 42, 592–597.
Wang, H.T., Dong, Z.X., Na, C.Z., 2013a. ACS Sustain. Chem. Eng. 1, 746–752.
Wang, J.L., Chen, G.H., Jiang, H., Li, Z.Y., Wang, X.M., 2013b. Analyst 138, 4427–4435.
Yick, S., Han, Z.J., Ostrikov, K., 2013. Chem. Commun. 49, 2861–2863.
Yin, P.T., Kim, T.H., Choi, J.W., Lee, K.B., 2013. Phys. Chem. Chem. Phys. 15, 12785–12799.
Yu, Y.Y., Chen, Z.G., He, S.J., Zhang, B.B., Li, X.C., Yao, M.C., 2014. Biosens. Bioelectron. 52, 147–152.
Zhang, Y.F., Xu, C.L., Li, B.X., Li, Y.B., 2013. Biosens. Bioelectron. 43, 205–210.
Zhou, H., Dong, J.H., Deo, V.K., Park, E.Y., Lee, J., 2013. Sens. Actuators B: Chem. 178, 192–199.
Zhou, H., Lee, J., Park, T.J., Lee, S.J., Park, J.Y., Lee, J., 2012. Sens. Actuators B: Chem. 163, 224–232.

Biosensors and Bioelectronics 58 (2014) 33–39

Contents lists available at ScienceDirect

Biosensors and Bioelectronics

journal homepage: www.elsevier.com/locate/bios

Metal enhanced fluorescence on nanoporous gold leaf-based assay platform for virus detection

Syed Rahin Ahmed [a,b], Md. Ashraf Hossain [b], Jung Youn Park [c], Soo-Hyung Kim [b], Dongyun Lee [d], Tetsuro Suzuki [e], Jaebeom Lee [d,*], Enoch Y. Park [a,f,**]

[a] Graduate School of Science and Technology, Shizuoka University, 836 Ohya Suruga-ku, Shizuoka 422-8529, Japan
[b] Department of Nano Fusion Technology, Pusan National University, Miryang 627-706, Republic of Korea
[c] National Fisheries Research and Development Institute, Busan 619-705, Republic of Korea
[d] Department of Nano Fusion Engineering and Cogno-Mechatronics Engineering, Pusan National University, Busan 609-735, Republic of Korea
[e] Department of Infectious Diseases, Hamamatsu University School of Medicine, 1-20-1 Higashi-ku, Handa-yama, Hamamatsu 431-3192, Japan
[f] Research Institute of Green Science and Technology, Shizuoka University, 836 Ohya Suruga-ku, Shizuoka 422-8529, Japan

ARTICLE INFO

Article history:
Received 11 October 2013
Received in revised form
26 January 2014
Accepted 15 February 2014
Available online 22 February 2014

Keywords:
Nanoporous gold leaf
Surface roughness
Fluorescence enhancement
Quantum dot
Influenza A virus

ABSTRACT

In the present study, a rapid, sensitive and quantitative detection of influenza A virus targeting hemagglutinin (HA) was developed using hybrid structure of quantum dots (QDs) and nanoporous gold leaf (NPGL). NPGL film was prepared by dealloying bimetallic film where its surface morphology and roughness were fairly controlled. Anti-influenza A virus HA antibody (ab66189) was bound with NPGL and amine ($-NH_2$) terminated QDs. These biofunctionalized NPGL and QDs formed a complex with the influenza virus A/Beijing/262/95 (H1N1) and the photoluminescence (PL) intensities of QDs were linearly correlated with the concentrations of the virus up to 1 ng/mL while no PL was observed in the absence of the virus, or in bovine serum albumin (BSA, 1 μg/mL) alone. In addition, it was demonstrated that this assay detected successfully influenza virus A/Yokohama/110/2009 (H3N2) that is isolated from a clinical sample, at a concentration of ca. 50 plaque forming units (PFU)/mL. This detection limit is 2-order more sensitive than a commercially available rapid influenza diagnostic test. From these results, the proposed assay may offer a new strategy to monitor influenza virus for public health.

1. Introduction

Epidemic diseases via transmission of the virus are becoming a threatening fear for public health system; e.g., the pandemic influenza A (H1N1) 2009 virus was firstly identified in Mexico in 2009 and caused rapid outbreaks, resulting in ca. 18,000 casualties around the world (Kawai et al., 2012; Panning et al., 2009). It continues to expand globally and causes significant rates of morbidity and mortality, particularly in the elderly and children. A rapid diagnosis of influenza viruses is vital for prevention and timely control of influenza epidemics. Currently forefront tests, i.e., immunosensors and genosensors for monitoring influenza viruses at initial stage usually require professional skill, equipment, multiple processes, and low sensitivity, resulting in retardation to clinical decision (Bonanni et al., 2010; Choi et al., 2010; Deng et al., 2011; Drexler et al., 2009; Druce et al., 2005; Egashira et al., 2008; Kok et al., 2010; Kukol et al., 2008; Owen et al., 2007; Pavlovic et al., 2008; Rahman et al., 2008; van Elden et al., 2001). Numerous technologies for higher sensitivity are emerging for virus detection.

In particular, it has been attractive to utilize photoluminescence (PL) enhancement based on the near-field plasmonic effect at metallic nanostructures (Driskell et al., 2011; Gramotnev and Bozhevolnyi, 2010; Schuller et al., 2010). The interaction between metal and semiconductor nanostructure offers attractive opportunities for tuning the optical properties of such composites based on exciton–plasmon coupling. Such composite structures feature complementary optical properties; e.g., semiconductor nanostructures give rise to high emission yields and light-harvesting capabilities, whereas the metallic surface is particularly effective for local probing, confined excitation, non-linear optics and intense PL enhancement (Achermann, 2010; Lee et al., 2006, 2007). Surface roughness has long been considered as one of the

* Corresponding author. Tel.: +82 55 350 5298; fax: +82 55 350 5299.
** Corresponding author at: Research Institute of Green Science and Technology, Shizuoka University, 836 Ohya Suruga-ku, Shizuoka 422-8529, Japan. Tel./fax: +81 54 238 4887.
E-mail addresses: rahin_sust@yahoo.com (S.R. Ahmed), ashraf3521@gmail.com (Md.A. Hossain), jypark@nfrdi.go.kr (J.Y. Park), sookim@pusan.ac.kr (S.-H. Kim), dlee@pusan.ac.kr (D. Lee), tesuzuki@hama-med.ac.jp (T. Suzuki), jaebeom@pusan.ac.kr (J. Lee), acypark@ipc.shizuoka.ac.jp, acypark@icloud.com (E.Y. Park).

http://dx.doi.org/10.1016/j.bios.2014.02.039
0956-5663

critical parameters for optimizing metal enhanced fluorescence and has enabled precise control of localized surface plasmon resonance (LSPR) as well as surface plasmon polariton (SPP). In rough metallic surface, the scattering of SPP mode can produce photons that can decrease diffraction limit and resolve the sub-wavelength structure, thereby unlocking the prospect of utilizing metal–semiconductor nanocomposite films for enhancing PL emission (Ahmed et al., 2012; Leong et al., 2010; Okamoto et al., 2004).

Nanoporous gold film has unique physical properties such as excellent stability, biocompatibility, as well as high specific surface area to form self-assembled monolayers from thiols, sulfides and disulfides (Biener et al., 2008; Huang and Sun, 2005). Usually a dealloying technique is utilized to prepare nanoporous structures with controlled pore size and ligaments. By exploiting the dealloying method, PL enhancement in the vicinity of metal nanostructures can be achieved with delicate control of the morphology of the surface on the scale of a few hundreds nanometers in conjunction with interconnected-porous structures (Ciesielski et al., 2008; Detsi et al., 2011).

In the present study, the fabrication of metallic surfaces with tunable roughness and controlled structures is reported using the dealloying method. The procedure for fabrication of metal–semiconductor hybrid nanostructures was achieved by means of self-assembly techniques, and the importance of the metallic surface morphology for PL enhancement is illustrated. Furthermore, this physical study expanded to develop a highly sensitive metal–semiconductor hybrid nanostructure for the detection of influenza virus (Fig. 1).

2. Materials and methods

2.1. Materials

3-Mercaptopropionic acid (MPA; 99%), poly-diallyldimethylammonium chloride (PDDA; M.W. 400,000–500,000), polyacrylic acid (PAA; M.W.,~450,000), cadmium perchlorate hydrate, thioglycolic acid (TGA), *N*-(3-dimethylaminopropyl)-*N*′-ethylcarbodiimide (EDC) and *N*-hydroxysuccinimide (NHS) were purchased from Sigma-Aldrich (Milwaukee, USA). Aluminum telluride (Al_2Te_3) was acquired from Cerac Company (Milwaukee, USA) at the highest purity available. The chromogenic substrate, 3,3′, 5,5′-tetramethylbenzidine (TMB) was obtained from Dojindo (Osaka, Japan). Gold leaf films were purchased from Giusto Manetti Inc. (Campi Bisenzio, Italy). Anti-Influenza A virus HA H1 antibody [B219M] (ab661189, Lot: GR40088-11), anti-Swine Influenza A (H1N1) HA antibody (ab91530, Lot: 942815), and anti-H3 (H3N2) antibody [InA227] (ab82454, Lot: GR84403-3) were purchased from Abcam Inc. (Cambridge, UK). Recombinant influenza A virus HA (H1N1) (New Caledonia/20/1999; Cat: 11683-V08H) and influenza virus A/Beijing/262/95 (H1N1) (Cat: 81N73-2) were purchased from Sino Biological Inc. (Beijing, China) and HyTest Lyd. (Turku, Finland), respectively. Influenza virus A/Yokohama/110/2009 (H3N2) that was isolated from a clinical sample was kindly provided by Dr. C. Kawakami of the Yokohama City Institute of Health, Japan, and was used for confirming the versatility of the assay system. ECL™ anti-mouse IgG, horseradish peroxidase (HRP) linked whole antibody (from sheep) was purchased from GE Healthcare UK Ltd. (Buckinghamshire, UK). All other chemicals were obtained from Wako Pure Chem. Ind. Ltd. (Osaka, Japan). All experiments were carried out using high purity deionized (DI) water (> 18 MΩ).

2.2. Preparation of NPGL and semiconductor nanoparticles

The dealloying process of NPGL film has previously been described (Ciesielski et al., 2008). In this study, a gold/silver leaf was gently placed on a microscope slide. This slide was then slowly immersed into a beaker of concentrated nitric acid in order to float the leaf at the air–acid interface. The glass slide was removed when the leaf floated freely on the surface of the nitric acid solution. Subsequently, it was dealloyed for the desired time intervals of 5, 10, 30, and 60 min, and labeled as NPGL05, NPGL10, NPGL30 and NPGL60, respectively. The leaf was removed from the acid using a glass slide and transferred into a beaker containing deionized water, where the leaf was rinsed by floating for 30 min. The dealloyed leaf was withdrawn on a glass substrate that had

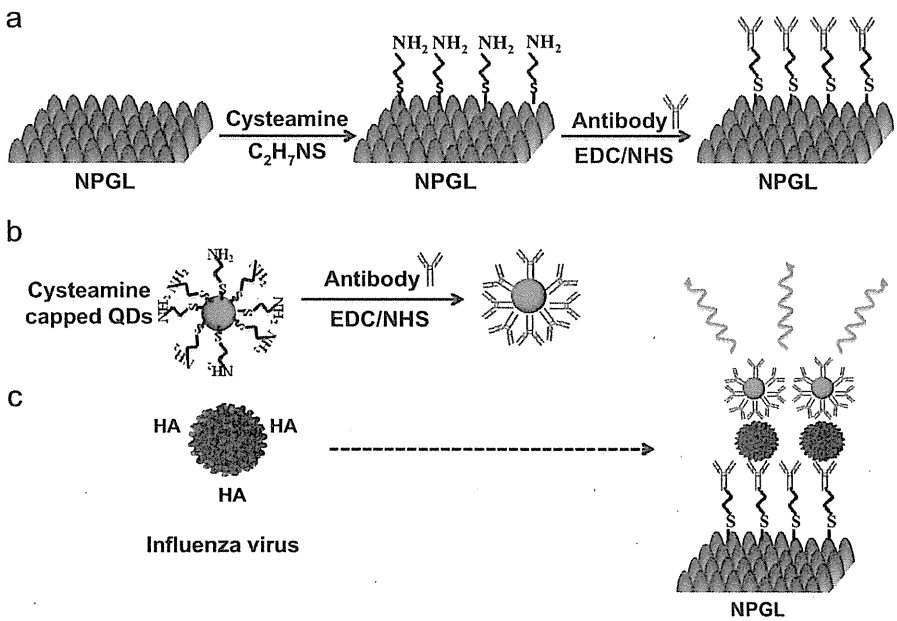

Fig. 1. Schematic of virus detection using nanoporous gold leaf (NPGL) film. The NPGL (a) and quantum dots (QDs) (b) were firstly conjugated with anti-hemagglutinin (HA) antibodies (anti-HA Ab, Y shape) by the reaction of ethylcarbodiimide (EDC)/*N*-hydroxysuccinimide (NHS). Then anti-HA Ab-conjugated with NPGL and QDs form complex (c) in presence of HA on the surface of influenza virus, finally enhancing PL intensity.

previously been modified with 3-mercaptopropyl trimethoxysilane in *n*-hexane. TGA-capped cadmium telluride (CdTe) QDs were also synthesized by a technique previously reported in detail (Gaponik et al., 2002) and stored at 4 °C prior to use.

2.3. Immobilization of CdTe QDs on the NPGL substrate

To evaluate optical properties of NPGL surface, the QDs were immobilized on the NPGL substrate by means of ultrasonic-assisted layer-by-layer (LbL) assembly (Ouyang et al., 2012; Perelshtein et al., 2008) (Supporting information S1). The polymer spacer layer of ca. 20 nm between nanocrystals and metal surface avoids unwanted quenching effects but assists PL enhancement.

2.4. Topographic observation and spectroscopic studies of NPGL films

Topographic images of the NPGL surfaces were obtained using atomic force microscopy (AFM, diInnova, Veeco, USA) and scanning electron microscopy (SEM, S4700, Hitachi High-Technol. Co., Minato-ku, Japan).

2.5. Detection platform of HA, Influenza viruses A/Beijing/262/95 (H1N1), and A/Yokohama/110/2009 (H3N2) on NPGL

Antibody specificity for HA (H1N1) was confirmed using an enzyme-linked immunosorbent assay (ELISA) (Supporting information S2) before conjugation to NPGL5 film. The anti-HA Ab (ab66189)-conjugated NPGL5 films (Supporting information S3) were rinsed 3 times with phosphate buffered saline (PBS). 100 μl anti-HA Ab-conjugated QDs (Ab-QDs) (Supporting information S1 and S4) containing different concentrations of recombinant influenza HA (H1N1) were added to the microplate wells. An Ab-QDs solution in BSA and without influenza virus HA (H1N1) was added to the same microplate as a negative control. To determine the PL enhancement effect of NPGL05 for HA detection, an identical amount of Ab-QDs solution containing 10 mg/mL HA protein was added to the wells of microplate. The microplate was then incubated for 30 min at room temperature. An infinite® F500 microplate fluorescence reader (TECAN, Männedorf, Switzerland) was employed to measure the PL intensity of each well. The samples were excited at 380 nm, and the exciting and the emission slits were 5 and 10 nm, respectively. Based on the PL values at different concentrations of HA, a dose-dependent curve was constructed. This NPGL-based assay platform was applied on detection of two different types of influenza viruses using the same protocol as described above. Influenza virus A/Beijing/262/95 (H1N1) was detected using anti-HA (H1N1) Ab-bioconjugated NPGL and QDs; influenza virus A/Yokohama/110/2009 (H3N2) was detected using anti-HA (H3N2) Ab-bioconjugated NPGL and QDs.

2.6. Detection of influenza virus by rapid influenza diagnostic test (RIDT)

To carry out direct and complementary comparison of the detection ability with commercially available influenza diagnostic kit, a commercial RIDT (ImunoAce Flu, TAUNS Lab. Inc., Numazu, Shizuoka, Japan), was purchased to detect Influenza virus A/Yokohama/110/2009 (H3N2) according to manufacturer's protocol. Different virus titers were prepared and then, three drops of virus solution were put on the sample port of the testing kit. Positive and negative influenza diagnostic results were obtained from different significant bands that appeared on the strip paper after 10 min of incubation at room temperature.

3. Results and discussion

3.1. Topographic observation of NPGL films

SEM and AFM images showed that the pore sizes of the substrates varied depending on the dealloying times (Fig. 2a–d). The size of the pores and ligaments increased with longer dealloying times due to increased removal of the less-noble constituent (silver) of the alloy. AFM was used to evaluate the root mean

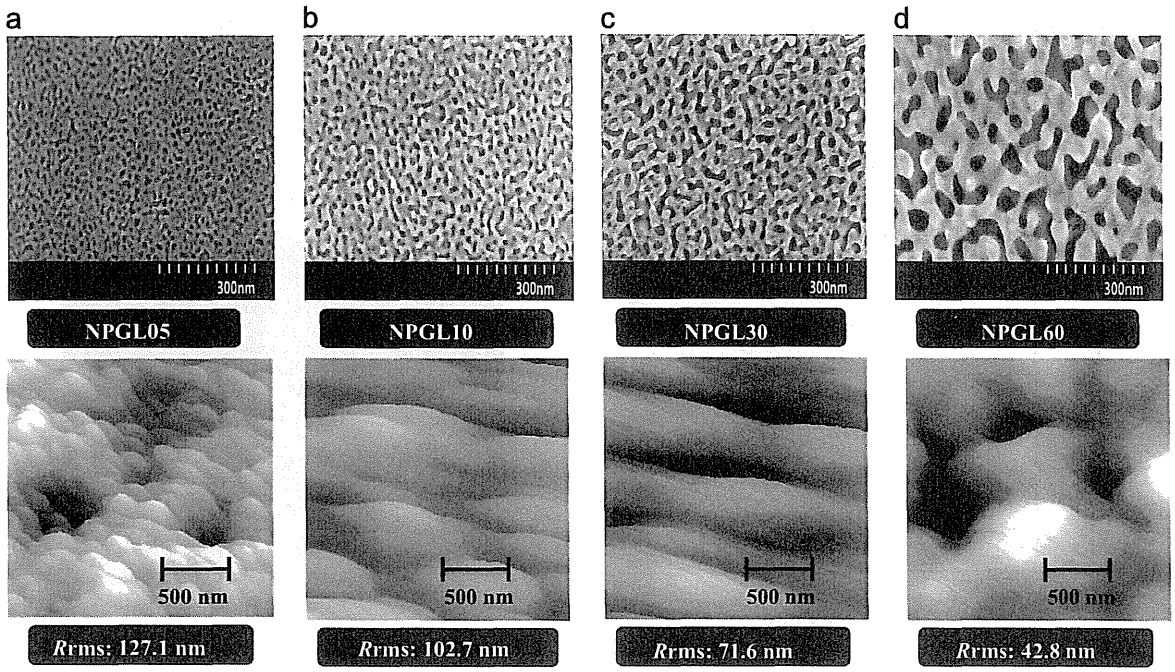

Fig. 2. SEM and AFM images and the measured R_{rms} of each NPGL sample with various dealloying times (5–60 min), where e.g., NPGL05 depicts 5 min of dealloying time. Dealloyed times are 5 min (a), 10 min (b), 30 min (c) and 60 min (d). Bars in upper and lower panels denote 300 and 500 nm respectively.

square roughness (R_{rms}) of the surface of each substrate with different dealloying times. The R_{rms} of the substrate was calculated in the scanning area ($3 \times 3\ \mu m^2$) of the AFM tip. It was found that the shorter is dealloying times the smaller is pore sizes, resulting in increasing surface irregularities and the surface roughness. Four selected NPGL samples of variant surface roughness (R_{rms} in lower panel of Fig. 2) were used for further optical evaluation.

3.2. Spectroscopic and microscopic studies of the NPGL films

The PL band of the synthesized QD solution was observed at 526 nm with a relative quantum yield of > 20% that was determined from the relative ratio versus rhodamine B dispersed in ethylene glycol, where the quantum yield of rhodamine B was 0.95 (Fig. S1A). Given that the surface roughness of each produced NPGL films differed, special care was taken in the QD immobilizing process to ensure that the equivalent amount of QDs was deposited on each substrate. Consequently, it is important to produce a monolayer of QDs on the surface of a metallic substrate. We monitored the absorbance of the QDs on the respective substrates to maintain similar intensities by adjusting the deposition time during the LbL process. Then, the PL intensity of the QD solution at the same absorption of the LbL film was measured. It was observed that the difference in the PL intensity of the various samples was less than 10%, indicating that fairly identical amount of QDs were deposited on the samples (Fig. S1B).

Indeed, PL enhancement of QDs on metal surfaces was observed. Fig. 3a shows that higher the roughness higher is the PL enhancement; e.g., the emission intensity of QDs on NPGL05 (R_{rms}=127.1 nm) and NPGL60 (R_{rms}=42.8 nm) was 9- and 2-fold higher than that on a glass substrate, respectively (Fig. 3a). When QDs were deposited on the metal surface without a spacer layer, no PL intensity was observed, rather quenching dominated. This remarkable PL enhancement may be attributed to a strong interaction with surface plasmon of metallic substrate. It has previously been reported that the excitons generated in the QDs can resonate with electron vibrations at the metal surface collectively to induce luminescence enhancement (Lee et al., 2004; Okamoto et al., 2006). Furthermore, the roughness effect on PL enhancement may be related to the multiple scattering phenomena of the SPP mode in combination with rough surfaces. Such roughness and imperfections in nanostructured random media allow SPP of high momentum to scatter and lose momentum and then couple to radioactive light (Okamoto et al., 2006). The fluorescence lifetimes (τ) of the respective samples were measured at an excitation wavelength of 380 nm using a light-emitting diode spectrophotometer (PTI Inc., USA). The spectra in Fig. 3b presents that the rougher the substrate is the shorter is the lifetime, i.e., the PL lifetime varied from 3.17 ns to 1.2 ns while the R_{rms} values varied from 42.8 to 127.1 nm (Fig. 3c). In contrast, the lifetime of CdTe QDs on glass slides was 7.42 ± 0.37 ns. In particular, the short dealloying time generated ultrafine structures that are characterized as small pores and pimples (< 10 nm) that play a major role in plasmonic scattering with consequent PL enhancement. Fig. 3d demonstrates a fluorescence microscopic image of the

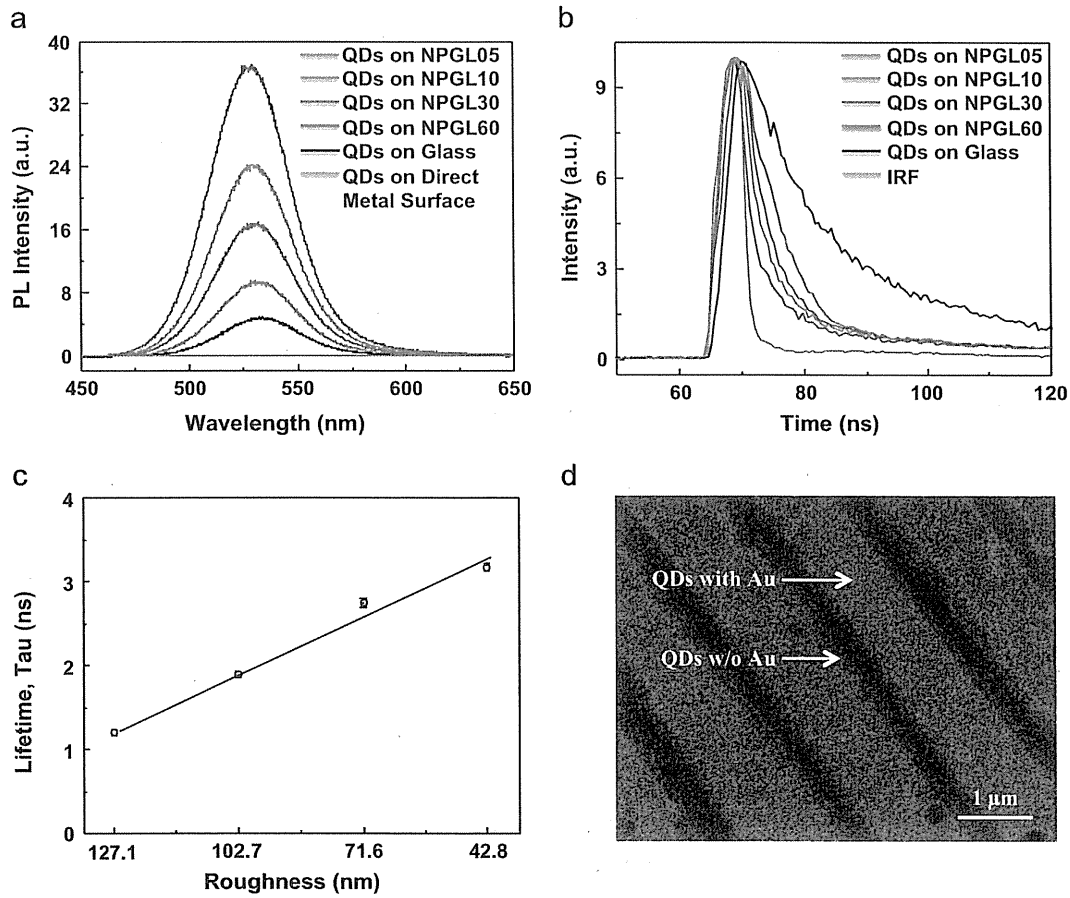

Fig. 3. (a) Photoluminescence (PL) spectra of QDs on different roughnesses of NPGL and glass substrate (for QD only); (b) time-based fluorescence kinetics profile of PL signal for QDs on different surfaces; (c) lifetimes (τ) variance depending on surface roughness; (d) fluorescence microscopic image of QDs on metallic nanostripe patterns. IRF in (b) stands for instrumental response function. The error bars in (c) indicate standard deviation (SD) in each measurement and the scale bar in (d) denotes 1 μm.

QD/polymer-deposited films on metallic nanostripe pattern to demonstrate strong PL enhancement induced by metal enhanced fluorescence. With increasing surface roughness, multiple scattering of lights occurs in nanostructured random media. The high enhancement effect observed in close proximity of metallic nanopatterns is primarily due to the absorption and/or emission bands of the QDs overlap with the scattering wavelength of the rough metallic surface. From these fundamental physical experiments NPGR05 substrate was chosen for further sensing experiments of virus detection.

3.3. Immunoassay of HA on NPGL05 and QDs

It is known that HA, a surface glycoprotein on the surface of viruses has unique immune-specificity in the initial stage of infection mechanism (Wiley and Skehel, 1987). The detailed optical observation at every respective step of bioconjugation with nanomaterials and antibodies was carefully monitored by using ELISA and FTIR spectrophotometry. Immuno-specificity of the anti-HA Ab (ab66189) for influenza virus A/Beijing/262/95 (H1N1) was investigated (Supporting information S1 and S2). A different type of Ab (ab91530) and BSA was used for comparison. A higher absorbance was observed with anti-HA Ab (ab66189) compared to the anti-HA Ab (ab91530) or BSA (Fig. S2A). From these experimental results, anti-HA Ab (ab66189) has a strong immune-specificity for influenza virus A/Beijing/262/95 (H1N1) whereas other antibody and BSA show no binding affinity with influenza A virus. The ELISA test indicated that the antibodies are successfully conjugated on the NPGLs without losing its binding affinity (Fig. S2B and C). Furthermore, FTIR bands found at 3700–3500 cm^{-1} for amide N–H stretching and 1690–1630 cm^{-1} for amide C=O stretching corresponds the chemical binding between NPGL and anti-HA Ab (ab66189) (Fig. S2D).

Then the same experiments were carried out to scrutinize any influence of binding affinity when cysteamine capped QDs were conjugated with anti-HA Ab (ab66189) using recombinant influenza H1N1 HA (New Caledonia/20/1999) (Fig. S3A), resulting that cysteamine capped QDs were successfully conjugated with the antibody (Fig. S3B and C). In fluorescence microscopic image, the aggregated and brighter spot might be virus deposited part on the film (Fig. S3D). The detection procedure consisted of three steps – (i) binding of antibody on NPGL, (ii) binding of antibody on QDs and (iii) immune-reaction between the antibody and antigen.

After confirming the binding affinity of antibody on the surface of NPGL film, the recombinant HA (H1N1) was monitored. Both NPGL film and QDs were bound with anti-HA (H1N1) Ab (ab66189). With HA, these bioconjugated components form a complex, consequently producing high PL intensity from QDs via surface plasmon resonance with the NPGL substrate. In our experiment, 3 times higher PL intensity were monitored in the nanostructure of the antibody-functionalized NPGL than that without the NPGL, where 10 μg/mL of HA was added in each experiment (Fig. 4A). In the quantitative analysis using different concentrations of HA, PL intensities were logarithmically correspondent on HA concentration in the range of 1 ng/ml–10 μg/mL (Fig. 4B and the inset). However, there was no significant PL change without any addition of HA or in the addition of BSA.

3.4. Immunoassay for virus detection

After confirmation of HA monitoring using this novel sensing system with NPGL and QDs, different concentrations of influenza virus A/Beijing/262/95 (H1N1) where the surface of this virus also has specific binding sites of anti-HA (H1N1) Ab were monitored. Similar results were observed as the previous experiment of HA only as shown in Fig. 4b. A significant PL enhancement was observed in the presence of viruses and NPGL (Fig. 5a). Furthermore, a logarithmical relationship existed between PL intensities and the virus concentration in the range of 1 ng/ml–10 μg/mL (Fig. 5b).

Using this developed monitoring system, an influenza virus A/Yokohama/110/2009 (H3N2) was monitored. The specificity of HA (H3N2) Ab 82454 for influenza virus A/Yokohama/110/2009 was confirmed (Fig. 5c), and binding of HA (H3N2) Ab 82454 with NPGL05 and QDs was also confirmed using ELISA (Fig. S4). Then, the sensitivity of influenza virus A/Yokohama/110/2009 (H3N2) detection was observed in the range of 50–10,000 plaque forming units (PFU)/mL (Fig. 5d). The detection limit was shown at ca. 50 PFU/mL.

3.5. Detection of influenza virus using rapid influenza diagnostic test (RIDT)

A commercially available RIDT kit (ImunoAce Flu, TAUNS Lab. Inc., Numazu, Shizuoka, Japan) was used for comparison with our sensing system to diagnose influenza virus infection using the influenza virus A/Yokohama/110/2009 (H3N2). Table 1 shows the results of the RIDT depending on the concentration of virus. In the case of the commercial RIDT, at least 5000 PFU/mL of virus was required for detection, which means the limit of detection (LOD) of the influenza virus detection using our sensing system of NPGL-QDs was 100 times more sensitive than that of the commercial RIDT (Fig. S5).

In this study, a new detection method on metallic surface based on exciton–plasmon interaction was presented. In particular, the

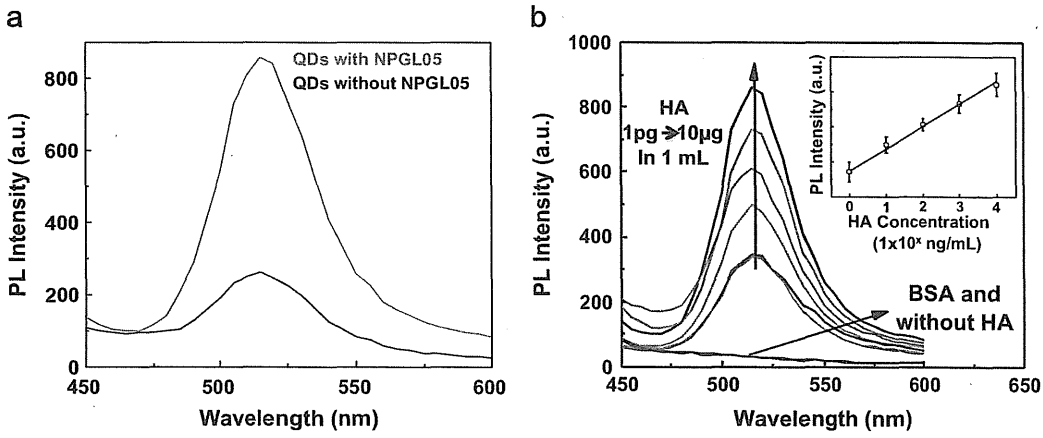

Fig. 4. (a) PL enhancement of QDs with and without the nanostructure; (b) PL enhancement corresponding on different quantities of recombinant influenza HA (H1N1) on anti-HA Ab-conjugated NPGL05. (Inset) The calibration curve of PL intensity versus HA concentration. The error bars indicate SD in each measurement.

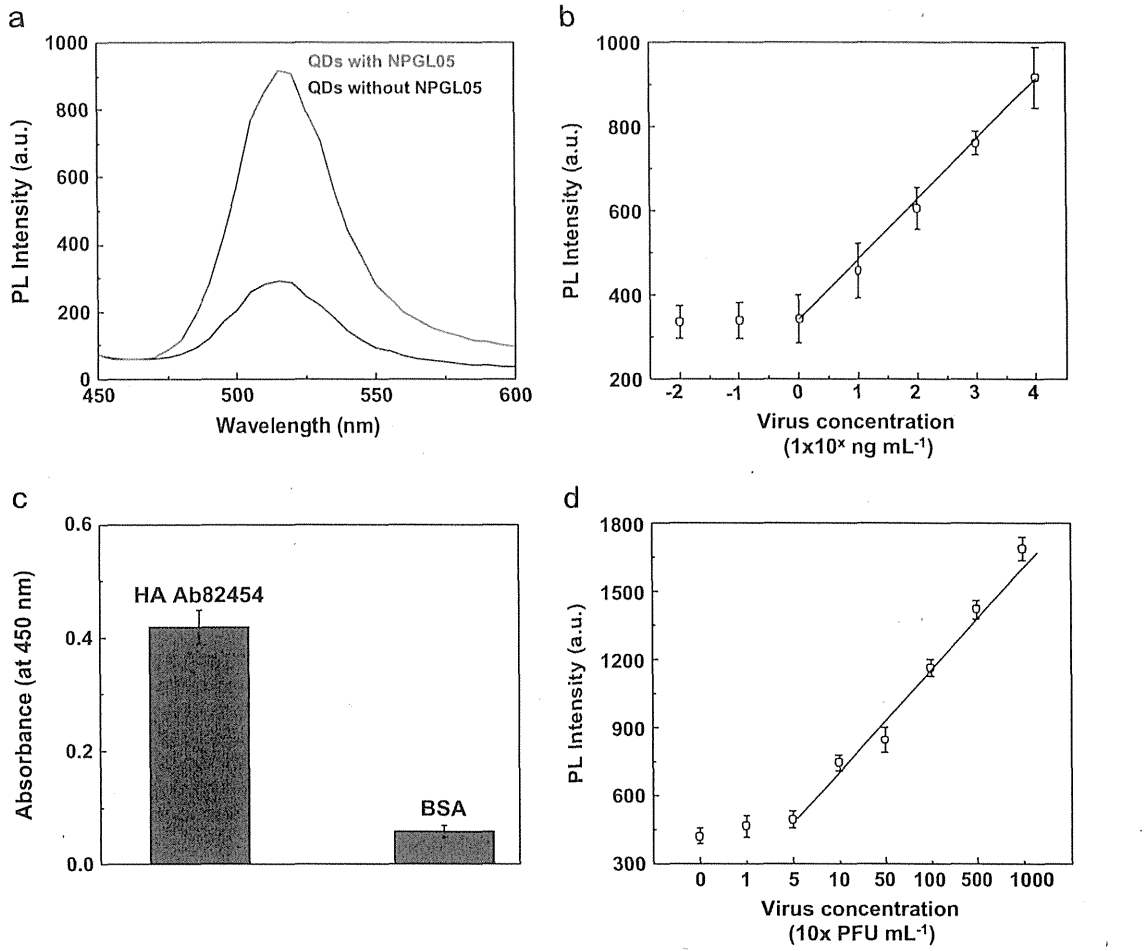

Fig. 5. (a) PL spectroscopic detection of influenza virus A/Beijing/262/95 (H1N1) using anti-HA (H1N1) Ab (ab66189)-bioconjugated QDs depending on the existence of anti-HA (H1N1) Ab (ab66189)-bioconjugated NPGL05 film; (b) PL intensity versus influenza virus A/Beijing/262/95 (H1N1) concentration; (c) ELISA results for anti-HA (H3N2) Ab 82454 binding with influenza virus A/Yokohama/110/2009 (H3N2); (d) the calibration curve of PL intensity corresponding on the concentration of the influenza virus A/Yokohama/110/2009 (H3N2). The error bars in (B–D) indicate SD (n=3).

Table 1
Comparison of influenza virus A/Yokohama/110/2009 (H3N2) detection using RIDT.

Detection method	Virus concentration (PFU/mL)								
	10,000	5000	1000	500	100	50	10	1	0
This study	+	+	+	+	+	+	−	−	−
Commercial RIDT	+	+	−	−	−	−	−	−	−

Note: + and − denote the positive and negative diagnoses, respectively.

research centered on the development of robust rough metallic surfaces that would be used for the generation of high efficient optical device for biosensor applications. Many implications for medical take care require a low detection system. An important goal here was to improve detection limit with high sensitivity. As we can see, our proposed detection method showed at least 100 times higher sensitivity than a representative commercial test kit. It might result from the presence of plasmonic rough metallic surface and adjacent control of distance between QDs to induce PL enhancement. In addition, the assay is performed with fewer amounts of reagents and easier to wash out unbound reagents. However, because of the lack of many medical samples, the huge analysis is not attainable using our technique up to now, which will be included in future work.

4. Conclusion

This paper reports a near-field optical evaluation of QDs and plasmonic surface composites with varying roughness. A dramatic enhancement of PL intensity and decay rate of the QDs was achieved on rougher metallic surfaces. The observation of these PL enhancements from nanocomposites was further applied for the development of sensitive influenza virus A (H1N1) detection (up to 1 ng/mL) and influenza A (H3N2) virus isolated from a clinical sample (up to 50 PFU/mL). The proposed method represented an alternative traditional method by requiring a higher sensitivity, much smaller sample volume, less amount reagents. Further research will be focused on the development of rough plasmonic metallic surface using self-assembly techniques as well as clinical evaluation.

Acknowledgments

We thank to Dr. Chiharu Kawakami of the Yokohama City Institute of Health, Japan, for providing influenza virus A/Yokohama/110/2009 (H3N2). This study was supported by a grant from the Korea Healthcare Technology R&D Project (A110191), the Ministry for Health, Welfare & Family Affairs, Republic of Korea;

by the National Fisheries Research & Development Institute (RP-2012-BT-030); by the Civil & Military Technology Cooperation Program through the National Research Foundation of Korea (NRF) funded by the Ministry of Science, ICT & Future Planning (No. 2013M3C1A9055407); and by the Financial Supporting Project of Long-term Overseas Dispatch of PNU's Tenure-track Faculty, 2011. This work was supported partly by Promotion of Nanobio-Technology Research to support Aging and Welfare Society from the Ministry of Education, Culture, Sports, Science and Technology, Japan. There was no additional external funding received for this study.

Appendix. Supporting information

Supplementary data associated with this article can be found in the online version at http://dx.doi.org/10.1016/j.bios.2014.02.039.

References

Achermann, M., 2010. J. Phys. Chem. Lett. 1, 2837–2843.
Ahmed, S.R., Cha, H.R., Park, J.Y., Park, E.Y., Lee, D., Lee, J., 2012. Nanoscale Res. Lett. 7, 438.
Biener, J., Nyce, G.W., Hodge, A.M., Biener, M.M., Hamza, A.V., Maier, S.A., 2008. Adv. Mater. 20, 1211–1217.
Bonanni, A., Pividori, M.I., del Valle, M., 2010. Analyst 135, 1765–1772.
Choi, Y.J., Kim, H.J., Park, J.S., Oh, M.H., Nam, H.S., Kim, Y.B., Cho, B.K., Ji, M.J., Oh, J.S., 2010. J. Clin. Microbiol. 48, 2260–2262.
Ciesielski, P.N., Scott, A.M., Faulkner, C.J., Berron, B.J., Cliffel, D.E., Jennings, G.K., 2008. ACS Nano 2, 2465–2472.
Deng, Y.M., Caldwell, N., Barr, I.G., 2011. PLoS One 6, e23400.
Detsi, E., Schootbrugge, M., Punzhin, S., Onck, P.R., Hosson, J.T.M.D., 2011. Scr. Mater. 64, 319–322.
Drexler, J.F., Helmer, A., Kirberg, H., Reber, U., Panning, M., Müller, M., Höfling, K., Matz, B., Drosten, C., Eis-Hübinger, A.M., 2009. Emerg. Infect. Dis. 15, 1662–1664.
Driskell, J.D., Jones, C.A., Tompkins, S.M., Tripp, R.A., 2011. Analyst 136, 3083–3090.
Druce, J., Tran, T., Kelly, H., Kaye, M., Chibo, D., Kostecki, R., Amiri, A., Catton, M., Birch, C., 2005. J. Med. Virol. 75, 122–129.
Egashira, N., Morita, S., Hifumi, E., Mitoma, Y., Uda, T., 2008. Anal. Chem. 80, 4020–4025.
Gaponik, N., Talapin, D.V., Rogach, A.L., Hoppe, K., Shevchenko, E.V., Kornowski, A., Eychmüller, A., Weller, H., 2002. J. Phys. Chem. B 106, 7177–7185.
Gramotnev, D.K., Bozhevolnyi, S.I., 2010. Nat. Photonics 4, 83–91.
Huang, J.F., Sun, I.W., 2005. Adv. Funct. Mater. 15, 989–994.
Kawai, Y., Kimura, Y., Lezhava, A., Kanamori, H., Usui, K., Hanami, T., Soma, T., Morlighem, J.E., Saga, S., Ishizu, Y., Aoki, S., Endo, R., Oguchi-Katayama, A., Kogo, Y., Mitani, Y., Ishidao, T., Kawakami, C., Kurata, H., Furuya, Y., Satito, Y., Okazaki, N., Chikahira, M., Hayashi, E., Tsuruoka, S., Toguchi, T., Saito, Y., Ban, T., Izumi, S., Uryu, H., Kudo, K., Sakai-Tagawa, Y., Kawaoka, Y., Hirai, A., Hayashizaki, Y., Ishikawa, T., 2012. PLoS One 7, e30236.
Kok, J., Blyth, C.C., Foo, H., Patterson, J., Taylor, J., McPhie, K., Ratnamohan, V.M., Iredell, J.R., Dwyer, D.E., 2010. J. Clin. Microbiol. 48, 290–291.
Kukol, A., Li, P., Estrela, P., Ko-Ferrigno, P., Migliorato, P., 2008. Anal. Biochem. 374, 143–153.
Lee, J., Govorov, A.X., Dulka, J., Kotov, N.A., 2004. Nano Lett. 4, 2323–2330.
Lee, J., Hernandez, P., Lee, J., Govorov, A.O., Kotov, N.A., 2007. Nat. Mater. 6, 291–295.
Lee, J., Javed, T., Skeini, T., Govorov, A.O., Bryant, G.W., Kotov, N.A., 2006. Angew. Chem. Int. Ed. 45, 4819–4823.
Leong, K., Chen, Y., Masiello, D.J., Zin, M.T., Hnilova, M., Ma, H., Tamerler, C., Sarikaya, M., Ginger, D.S., Jen, A.K.Y., 2010. Adv. Funct. Mater. 20, 2675–2682.
Okamoto, K., Vyawahare, S., Scherer, A., 2006. J. Opt. Soc. Am. B 23, 1674–1678.
Okamoto, K., Niki, I., Shvartser, A., Narukawa, Y., Mukai, T., Scherer, A., 2004. Nat. Mater. 3, 601–605.
Ouyang, J., Chang, M., Zhang, Y., Li, X., 2012. Thin Solid Films 520, 2994–2999.
Owen, T.W., Al-Kaysi, R.O., Bardeen, C.J., Cheng, Q., 2007. Sens. Actuators B – Chem. 126, 691–699.
Panning, M., Eickmann, M., Landt, O., Monazahian, M., Ölschläger, S., Baumgarte, S., Reischl, U., Wenzel, J.J., Niller, H.H., Günther, S., 2009. Eurosurveillance 14, 2003–2008.
Pavlovic, E., Lai, R.Y., Wu, T.T., Ferguson, B.S., Sun, R., Plaxco, K.W., Soh, H.T., 2008. Langmuir 24, 1102–1107.
Perelshtein, I., Applerot, G., Perkas, N., Guibert, G., Mikhailov, S., Gedanken, A., 2008. Nanotechnology 19, 245705–245710.
Rahman, M., Vandermause, M.F., Kieke, B.A., Belongia, E.A., 2008. Diagn. Microbiol. Infect. Dis. 62, 162–166.
Schuller, J.A., Barnard, E.S., Cai, W., Jun, Y.C., White, J.S., Brongersma, M.L., 2010. Nat. Mater. 9, 193–204.
van Elden, L.J., van Essen, G.A., Boucher, C.A., van Loon, A.M., Nijhuis, M., Schipper, P., Verheij, T.J., Hoepelman, I.M., 2001. Br. J. Gen. Pract. 51, 630–634.
Wiley, D.C., Skehel, J.J., 1987. Ann. Rev. Biochem. 56, 365–394.

JVI
Journals.ASM.org

Hallmarks of Hepatitis C Virus in Equine Hepacivirus

Tomohisa Tanaka,[a] Hirotake Kasai,[a] Atsuya Yamashita,[a] Kaori Okuyama-Dobashi,[a] Jun Yasumoto,[a] Shinya Maekawa,[b] Nobuyuki Enomoto,[b] Toru Okamoto,[c] Yoshiharu Matsuura,[c] Masami Morimatsu,[d] Noboru Manabe,[e] Kazuhiko Ochiai,[f] Kazuto Yamashita,[g] Kohji Moriishi[a]

Department of Microbiology, Faculty of Medicine, University of Yamanashi, Yamanashi, Japan[a]; First Department of Internal Medicine, Faculty of Medicine, University of Yamanashi, Yamanashi, Japan[b]; Department of Molecular Virology, Research Institute for Microbial Diseases, Osaka University, Osaka, Japan[c]; Laboratory of Laboratory Animal Science and Medicine, Department of Disease Control, Graduate School of Veterinary Medicine, Hokkaido University, Sapporo, Japan[d]; Animal Resource Science Center, Graduate School of Agricultural and Life Sciences, The University of Tokyo, Kasama, Japan[e]; Department of Basic Science, School of Veterinary Nursing and Technology, Faculty of Veterinary Science, Nippon Veterinary and Life Science University, Tokyo, Japan[f]; Department of Small Animal Clinical Sciences, School of Veterinary Medicine, Rakuno Gakuen University, Ebetsu, Hokkaido, Japan[g]

ABSTRACT

Equine hepacivirus (EHcV) has been identified as a closely related homologue of hepatitis C virus (HCV) in the United States, the United Kingdom, and Germany, but not in Asian countries. In this study, we genetically and serologically screened 31 serum samples obtained from Japanese-born domestic horses for EHcV infection and subsequently identified 11 PCR-positive and 7 seropositive serum samples. We determined the full sequence of the EHcV genome, including the 3′ untranslated region (UTR), which had previously not been completely revealed. The polyprotein of a Japanese EHcV strain showed approximately 95% homology to those of the reported strains. HCV-like *cis*-acting RNA elements, including the stem-loop structures of the 3′ UTR and kissing-loop interaction were deduced from regions around both UTRs of the EHcV genome. A comparison of the EHcV and HCV core proteins revealed that Ile^{190} and Phe^{191} of the EHcV core protein could be important for cleavage of the core protein by signal peptide peptidase (SPP) and were replaced with Ala and Leu, respectively, which inhibited intramembrane cleavage of the EHcV core protein. The loss-of-function mutant of SPP abrogated intramembrane cleavage of the EHcV core protein and bound EHcV core protein, suggesting that the EHcV core protein may be cleaved by SPP to become a mature form. The wild-type EHcV core protein, but not the SPP-resistant mutant, was localized on lipid droplets and partially on the lipid raft-like membrane in a manner similar to that of the HCV core protein. These results suggest that EHcV may conserve the genetic and biological properties of HCV.

IMPORTANCE

EHcV, which shows the highest amino acid or nucleotide homology to HCV among hepaciviruses, was previously reported to infect horses from Western, but not Asian, countries. We herein report EHcV infection in Japanese-born horses. In this study, HCV-like RNA secondary structures around both UTRs were predicted by determining the whole-genome sequence of EHcV. Our results also suggest that the EHcV core protein is cleaved by SPP to become a mature form and then is localized on lipid droplets and partially on lipid raft-like membranes in a manner similar to that of the HCV core protein. Hence, EHcV was identified as a closely related homologue of HCV based on its genetic structure as well as its biological properties. A clearer understanding of the epidemiology, genetic structure, and infection mechanism of EHcV will assist in elucidating the evolution of hepaciviruses as well as the development of surrogate models for the study of HCV.

The *Flaviviridae* family is composed of four genera: *Flavivirus*, *Pestivirus*, *Pegivirus*, and *Hepacivirus*. *Flaviviridae* family viruses are enveloped and contain a single-stranded, positive-sense RNA genome, which encodes a single large precursor polyprotein composed of approximately 2,800 to 3,000 amino acids. The genus *Hepacivirus* had included only two species, hepatitis C virus (HCV) and GB virus B (GBV-B), until 2010. GBV-B was isolated from serum samples obtained from laboratory tamarins by 11 passages of serum obtained from a human patient with idiopathic hepatitis (1). Although GBV-B experimentally infects tamarins and common marmosets, but not chimpanzees, *in vivo* (2, 3), the natural host of GBV-B has not yet been clarified. Several hepacivirus species were recently detected in dogs, horses, bats, and rodents and tentatively designated nonprimate hepaciviruses (NPHVs). Bat hepaciviruses have been isolated from some species of bats in Kenya (4), while rodent hepaciviruses have been isolated from several species of rodents in Germany, the Netherlands, South Africa, and Namibia (5, 6). GBV-B is phylogenetically more similar to rodent hepacivirus than to HCV (5). Several strains of equine hepacivirus (EHcV) have been isolated from domestic horses in the United States, the United Kingdom, and Germany (5, 7, 8). The canine hepacivirus was isolated from dogs in the United States (9) but has not yet been genetically or serologically detected in any dogs other than those from the first report (5, 7, 8). The polypeptides of canine hepacivirus show approximately 95% amino acid homology to those of the EHcV strains, suggesting that canine hepacivirus may belong to the same species as EHcV and

Received 8 August 2014 Accepted 2 September 2014
Published ahead of print 10 September 2014
Editor: T. S. Dermody
Address correspondence to Kohji Moriishi, kmoriishi@yamanashi.ac.jp.

doi:10.1128/JVI.02280-14

that infections may be rare in dogs (5, 7, 8, 10). Recent phylogenetic analyses identified EHcV as the most closely related viral homologue of HCV among the reported NPHV strains; however, epidemiological and virological information on EHcV is limited. The open reading frames of EHcV strains show approximately 95% homology to one another, suggesting that previously reported EHcV strains may be classified into one species. Several genome sequences of rodent hepacivirus have already been completely determined (5). The 3′ untranslated region (UTR) of HCV was found to include three stem-loop (SL) structures, while variable stem-loop structures were found in that of rodent hepacivirus and GBV-B (5). However, the nucleotide sequence of the EHcV 3′ UTR has not yet been determined completely because the adenine-rich [(A)-rich] sequence downstream of the stop codon in the EHcV genome interrupts an ordinary 3′-rapid amplification of cDNA ends (RACE) reaction (8). The RNA secondary structure of the hepacivirus 3′ UTR may indicate species specificity (5).

On the basis of amino acid similarities among the polyproteins of NPHVs and HCV, the N-terminal one-fourth of the NPHV polyprotein has been predicted to be cleaved by signal peptidase into mature structural proteins and a viroporin (core, E1, E2, and p7), while the C-terminal three-fourths has been predicted to be cleaved by viral proteases into maturated nonstructural proteins (NS2, NS3, NS4A, NS4B, NS5A, and NS5B) (6). Core, E1, and E2 have been predicted to form viral particles with host lipids, although it remains unclear whether p7 is incorporated into a viral particle. Signal peptide peptidase (SPP) was shown to further cleave the C-terminal transmembrane region of HCV and GBV-B core protein after signal peptidase-dependent cleavage (11, 12). However, whether SPP cleaves the C-terminal transmembrane region of the NPHV core protein remains unknown.

The mature core proteins of HCV and GBV-B are localized mainly on lipid droplets (LDs) (13, 14). The core proteins of dengue virus are also localized on LDs but are not cleaved by SPP (15), suggesting that localization of the core protein on LDs may be one of the common characteristics of the *Flaviviridae* family. The HCV core protein is known to be partially localized in the detergent-resistant membrane (DRM), which originates from lipid raft-like membranes (16, 17). The DRM is composed of cholesterol and sphingolipids, which are included in the replication compartment known as the membranous web (18, 19). Therefore, LDs and DRM are considered to be the intracellular compartments for the replication and viral assembly of HCV, but it is currently unknown whether NPHV core proteins are localized on LDs and DRM.

Epidemiological information on EHcV is still limited. The results of the present study demonstrated that Japanese-born domestic horses were infected with EHcV, which showed high homology to the reported strains on the basis of its nucleotide and amino acid sequences. We predicted the RNA secondary structures around the 5′ and 3′ UTRs of the EHcV genome and analyzed the biological properties of the EHcV core protein in relation to the HCV core protein.

MATERIALS AND METHODS

Samples. Serum samples 1 to 13 were collected from Japanese-born domestic horses raised on one farm, farm A, located in Hokkaido, Japan, while groups of serum samples numbered 14 to 18 and 19 to 31 were from horses on farms B and C, respectively, located in Tokyo, Japan (Fig. 1). The distance between Hokkaido and Tokyo is about 1,000 km. All sample collections conformed to guidelines for the care and use of laboratory animals (Yamanashi University) and were approved by the Institutional Committee of Laboratory Animal Experimentation (Yamanashi University). All samples were divided into small aliquots and stored at −80°C until nucleic acid extraction.

RT-PCR. Total RNAs were prepared from horse sera using a Qiagen viral RNA extraction kit (Qiagen, Valencia, CA). RNAs were converted to cDNA using a PrimeScript reverse transcription-PCR (RT-PCR) kit (TaKaRa, Shiga, Japan) with random primers. The viral gene was amplified by PCR using PuReTaq Ready-To-Go PCR beads (GE Healthcare, Piscataway, NJ) with three pairs of primers: NPHV-F1 (5′-TGTCACCT ACTATCGGGG-3′) and NPHV-R1 (5′-TCAAGCCTATACAGCAAAG G-3′), NPHV-F2 (5′-ATCATTTGTGATGAGTGCC-3′) and NPHV-R2 (5′-CATAAGGGCGTCCGTGGC-3′), and NPHV-F3 (5′-GTGGTCGCC ACGGATGCC-3′) and NPHV-R3 (5′-ACCCTATGAAGACGCTCTCC-3′). PCR was carried out as follows: one cycle at 92°C for 5 min; 35 repeats of one cycle at 94°C for 0.5 min, 58°C for 0.5 min, and 72°C for 0.5 min, in that order; and one cycle at 72°C for 1 min followed by holding at 4°C. The PCR products were electrophoresed on 1.5% agarose gels, stained with ethidium bromide, and visualized using the BioDoc-It imaging system (UVP, Upland, CA).

Determination of the EHcV genomic sequence. The viral genome of EHcV was segmentally amplified by PCR using the primers listed in Table 1. The PCR products were cloned into T vectors prepared from pBluescript II SK(−) (20). The DNA sequences of the PCR products were determined using an ABI Prism BigDye Terminator version 1.1 cycle sequencing kit and an ABI Prism 310 genetic analyzer (Life Technologies, Tokyo, Japan). More than three colonies were picked up among the transformants of *Escherichia coli* with regard to the accuracy of the sequence. The nucleotide sequences of the PCR products were determined in forward and reverse directions. The junction of two adjacent PCR products was confirmed by PCR using primers that overlapped two close regions. The 5′-terminal sequence upstream of the open reading frame was determined with a 5′-RACE core set (TaKaRa) using the 5′ phospholyrated RT primer for the NPHV 5′ UTR (5′-CATCCTATCAGACCG-3′). The 3′-terminal region downstream of the (A)-rich region was determined by the 3′-RACE method (21, 22), modified as follows: Total RNAs were prepared from horse serum using TRIzol LS reagent (Invitrogen, Carlsbad, CA) with 40 μg of glycogen (Nacalai Tesque, Kyoto, Japan). The poly(U) tail was added to the 3′ end of the RNA preparation using *Escherichia coli* poly(U) polymerase (New England BioLabs, Ipswich, MA) and was incubated for 45 min at 37°C. The resulting preparation was reverse transcribed by the SuperScript First-Strand Synthesis system (Life Technologies) using an oligo(dA) adapter primer (5′-TTGCGAGCACAGAATTAATACG ACTCACAAAAAAAAAAAAVN-3′). The sequence of each region was determined by sequencing more than 3 clones. The primers for PCR amplification and the RACE methods are listed in Table 1. The whole sequence of the EHcV strain isolated from serum sample 3 (GenBank accession number AB863589) was determined by the method described above. The EHcV strain was designated JPN3/JAPAN/2013 in this study. The partial NS5B-coding regions and 3′ UTRs were amplified from serum samples 5 and 1. The nucleotide sequences of samples 5 and 1 (GenBank accession numbers AB921150 and AB921151, respectively) were determined by the method described above. The neighbor-joining trees of the nucleotide sequences from the NPHV, HCV, and GBV-B strains were predicted by the method of Saitou et al (23). Trees were constructed by the maximum composite likelihood method calculated by using the program MEGA5 (24) (see Fig. 3). The secondary protein structures were predicted by the method of Garnier et al. (25) (see Fig. 6). Hydrophobicity plots of the EHcV and HCV core proteins were prepared by the method of Kyte and Doolittle (26) and drawn using the software Genetyx (Nihon Genetyx, Tokyo, Japan) (see Fig. 5).

Quantification of viral genomic RNAs in horse sera. Total RNA was prepared from equine serum using a Qiagen viral RNA extraction kit and was then reverse transcribed into cDNA by using a PrimeScript RT-PCR

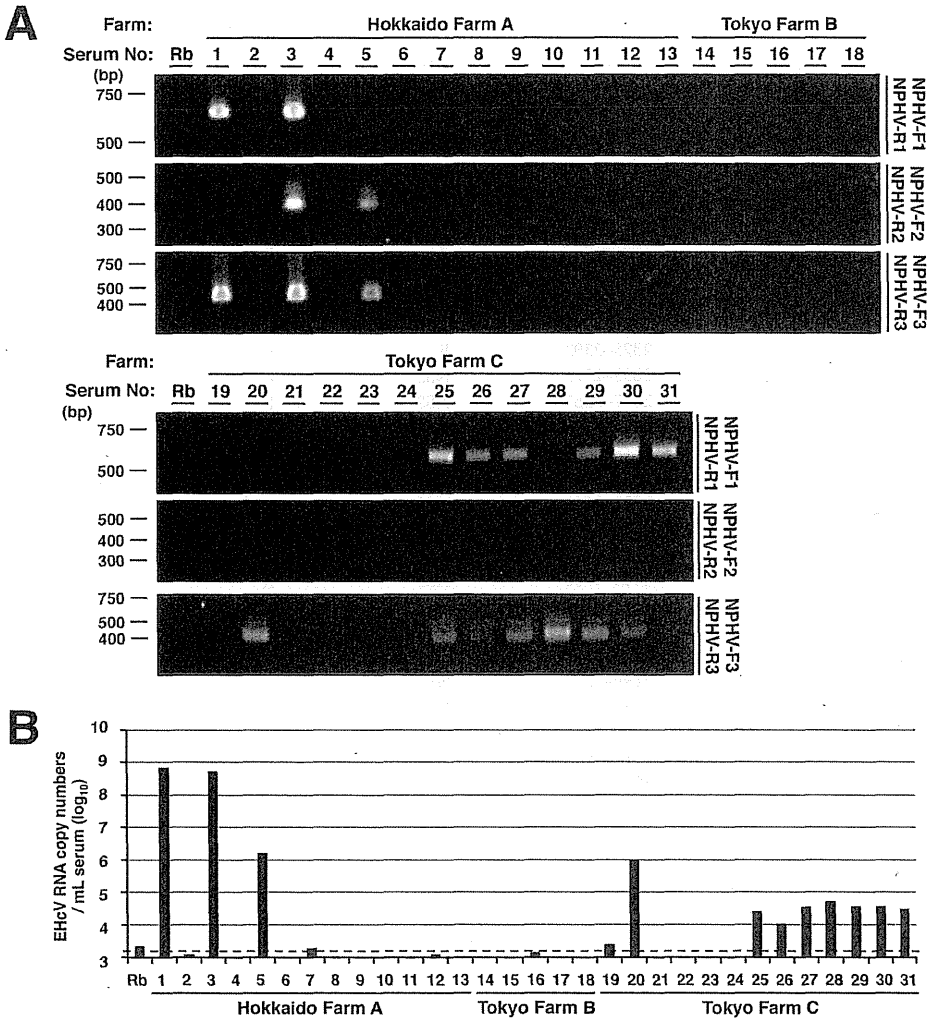

FIG 1 Detection and genetic analyses of NPHV genomic RNA in sera of Japanese domestic horses. (A) Total RNAs extracted from 31 equine sera and normal rabbit serum (Rb) as a negative control were subjected to RT-PCR analysis. Hokkaido Farm A, Tokyo Farm B, and Tokyo Farm C indicate the farms where the individual horses were reared. Three sets of primers, NPHV-F1 and NPHV-R1, NPHV-F2 and NPHV-R2, and NPHV-F3 and NPHV-R3, were used to amplify NPHV-specific gene regions. The PCR products were electrophoresed and stained with ethidium bromide. (B) Total RNAs were isolated from sera, reverse-transcribed, and estimated as a copy number per ml. Normal rabbit serum was used as a negative control. The dashed line indicates the cutoff level.

kit with random primers. The amount of targeted viral RNA was estimated using SYBR GreenER qPCR SuperMix (Life Technologies) and the ABI StepOnePlus real-time PCR system (Life Technologies). The region encoding NS3 was targeted with the primer pair NPHV-F3 (5′-GTGGTC GCCACGGATGCC-3′) and NPHV-R3 (5′-ACCCTATGAAGACGCTC TCC-3′). Total RNAs extracted from conventional rabbit serum were used as a negative control to determine the analytical threshold line. The *in vitro*-transcribed RNA of EHcV was utilized for the standard curve.

Prediction of RNA secondary structures. The 5′-UTR sequences of EHcV strains were aligned with the MUSCLE program and subjected to a manual search for covariant nucleotide substitutions. The RNA folding structure upstream of domain III in the 5′ UTR was predicted using the Mfold web server (27) with conventional phylogenetic conservation analysis due to the lack of sufficient homology to the 5′ UTR sequences of HCV strains. The NS5B-coding regions and 3′ UTRs of EHcV strains were aligned with the program MUSCLE. Conserved secondary structures were predicted as described above. The secondary structures of the 3′ UTR in EHcV were predicted by the Mfold web server without confirming phylogenetic data because of the absence of additional available sequences of the EHcV 3′ UTR and the lack of sufficient homology to the HCV X-tail sequences.

Plasmids. The PCR product encoding the EHcV core protein was amplified from serum sample 3 and was then cloned into the BamHI and XhoI sites of pcDNA3.1-Flag/HA, which encodes the FLAG and hemagglutinin (HA) epitope tags, as reported previously (28). Ala^{204} was replaced with Lys to prevent signal peptidase-dependent cleavage. The translated EHcV core protein was added to the FLAG and HA epitope tags at the N and C termini (EHcVc), respectively. A point mutation was generated using a KOD mutagenesis kit (Toyobo, Osaka, Japan). The PCR products encoding EHcVc or the mutant in which Ile^{190} and Phe^{191} were replaced with Ala and Leu (EHcVc-mt), respectively, were introduced into the AflII and EcoRV sites of pCAGGS using an In-Fusion HD cloning kit (TaKaRa). The introduced fragments of all plasmids were confirmed by sequencing using an ABI Prism 310 genetic analyzer (Applied Biosystems). The plasmid encoding the N-terminally FLAG-tagged and C-terminally HA-tagged HCV core protein (HCVc) and the mutant in which

TABLE 1 List of PCR primers used in this study

Primer	Nucleotide position	Genome location	F or R[a]	Sequence (5′→3′)
Primer for cloning of the NPHV genome	92–111	5′ UTR	F	ATGTGTCACTCCCCCTATGG
	367–386	5′ UTR	R	CTATGGTCTACGAGACCGGC
	268–285	5′ UTR	F	AGCCGAAATTTGGGCGTG
	1207–1224	E1	R	AAACAGAAGCCATAGCGG
	1116–1132	E1	F	AGTGCTTGTTGGGTGCC
	1697–1713	E2	R	GTCCTTTGCACTTCGGG
	1605–1623	E2	F	ACTGTTAAGCAGATGTGGG
	2103–2121	E2	R	CACAGAGTTGGTAAGTAGC
	2007–2023	E2	F	AAGCAGTGTGGTGCTCC
	2526–2545	E2	R	AAACAGAACCAGAGAATTGC
	2375–2392	E2	F	CCCTGCCTTCACTACTGG
	2898–2913	NS2	R	CGAGATAGCGCCAAGC
	2847–2867	NS2	F	TTTATGCTAGTAAAGTGGTGG
	3396–3415	NS2	R	GGTGATAAAAGTCTCCATCC
	3318–3334	NS2	F	ATCCTCCATGGCTTGCC
	3819–3835	NS3	R	GGGCCACCTGAACTACC
	3732–3750	NS3	F	ACCAGGACGGGTCAGGTCG
	4254–4270	NS3	R	ATAATGTCATAAGCACC
	4177–4195	NS3	F	CTAGTTGCAAGACAACGGG
	4682–4700	NS3	R	AGTGTTGCAGTCAGTGACG
	4574–4591	NS3	F	TGTCACCTACTATCGGGG
	5199–5218	NS3	R	TCAAGCCTATACAGCAAAGG
	4574–4591	NS3	F	TGTCACCTACTATCGGGG
	5199–5218	NS3	R	TCAAGCCTATACAGCAAAGG
	5134–5152	NS3	F	CTCCCAGCAAAGATGAACG
	5997–6014	NS4B	R	AGCACCCACACCAACAGC
	5919–5934	NS4B	F	AAGATCTTGAGTGGTG
	6651–6632	NS5A	R	GCCGATAACTCTGACAGC
	6547–6564	NS5A	F	ACACCTGGAAAACAGCCG
	7293–7310	NS5A	R	AGATTCCGTGGCCGAAGG
	7235–7252	NS5A	F	AGCTCTCGTTTCCGGGTG
	7573–7590	NS5B	R	TAGCTGACGCTGTTGTGG
	7511–7527	NS5B	F	ACGCCACCCTATAGGCC
	8027–8046	NS5B	R	GTTGACGGGGAGTGTATTGG
	7926–7943	NS5B	F	ATCGTTTACCCCGATTTG
	8528–8545	NS5B	R	CAAGATGTTATCTGCTCC
	8457–8474	NS5B	F	CGTGACTTCACTAATGCC
	9069–9086	NS5B	R	GTCAATCGAGTTTACGCC
Primer for 5′ RACE	235–252	5′ UTR	F	AATCGCGGCTTGAACGTC
	213–230	5′ UTR	R	TGTACTCACGGATTCACG
Primer for 3′ RACE	8979–8999	NS5B	F	CTTAAAGTACGTGGTGGTCGC
Adapter primer			R	GCGAGCACAGAATTAATACGAC

[a] F, forward; R, reverse.

Ile[176] and Phe[177] were replaced with Ala and Leu (HCVc-mt), respectively, were described previously (28). The gene encoding human signal peptide peptidase (SPP) or its mutant was introduced into pcDNA3.1-myc/His C (Invitrogen) instead of the plasmids described previously (28). The resulting plasmids encoded C-terminally myc-$His_{\times 6}$-tagged wild-type SPP (SPP-wt) or the mutant protein in which Asp[219] was replaced with Ala (SPP-D219A).

Cell culture and transfection. The human embryonic kidney cell line 293FT and the human hepatoma cell line Huh7OK1 (29) were maintained in Dulbecco's modified Eagle's minimal essential medium (DMEM) supplemented with 100 U/ml penicillin, 100 μg/ml streptomycin, nonessential amino acids (Sigma, St. Louis, MO), sodium pyruvate (Sigma), and 10% fetal bovine serum (FBS) and were then cultured at 37°C under the conditions of a humidified atmosphere and 5% CO_2. Plasmids were transfected into cell lines using XtremeGene 8 (Roche) according to the manufacturer's protocol.

Western blot analysis. 293FT cells were cultured in 6-well plates and transfected with the appropriate plasmids. The transfected cells were harvested at 18 h posttransfection, washed with cold phosphate-buffered saline (PBS), and suspended in 50 μl of the lysis buffer consisting of 20 mM Tris-HCl (pH 7.5), 135 mM NaCl, 10% glycerol, 1% Triton X-100, and protease inhibitor cocktail (Merck Bioscience, Calbiochem, San Diego, CA). The lysates were centrifuged at 19,000 × *g* for 5 min at 4°C. The supernatants were mixed with 16 μl of 4× SDS sample buffer and then boiled at 60°C for 20 min. The resulting mixtures were subjected to SDS-PAGE. The proteins in a gel were transferred to polyvinylidene difluoride (PVDF) membranes and incubated with mouse anti-FLAG antibodies (Sigma), mouse anti-HA antibodies (Covance, Princeton, NJ), mouse

anti-c-*myc* antibodies (BD Pharmingen, San Diego, CA), or mouse anti-beta-actin antibodies (Santa Cruz Biotechnology, Santa Cruz, CA) and were then incubated with the appropriate horseradish peroxidase (HRP)-conjugated secondary antibodies. Immunocomplexes were visualized with SuperSignal West Femto substrate (Thermo Scientific, Rockford, IL) and detected using an LAS-4000 Mini image analyzer (GE Healthcare, Buckinghamshire, United Kingdom).

Detection of antibodies against EHcV. To detect anti-EHcV antibodies in horse sera, we subjected lysates prepared from 293FT cells expressing EHcVc, which is an N-terminally FLAG-tagged and C-terminally HA-tagged EHcV core protein (a positive reference), or cells transfected with an empty plasmid (a negative reference) to Western blotting, as described above. The resulting PVDF membranes were incubated with Blocking One solution (Nacalai Tesque) for blocking at room temperature for 30 min and then incubated with 1,000-fold-diluted horse serum in 10-fold-diluted Blocking One. Mouse anti-FLAG or rabbit anti-EHcV core antibody was used as a positive serum control. The resulting membrane was incubated with an HRP-conjugated antibody to mouse, rabbit, or horse IgG (Abcam, Cambridge, UK) at room temperature for 1 h. Protein bands with a molecular mass of 28 kDa were detected in the positive reference, but not in the negative reference, using positive serum or an antibody to the FLAG epitope tag or EHcV core protein. The rabbit polyclonal antibody against the EHcV core protein was generated by immunization using peptides of the residues from 2 to 15, GNKSKNQKPQPQRG (Scrum Inc., Tokyo, Japan).

Pulldown assay for SPP binding. Human embryonic kidney 293FT cells expressing EHcVc or HCVc with or without SPP-D219A were harvested at 18 h posttransfection, washed with cold PBS, suspended in 100 μl of the lysis buffer, and centrifuged at 14,000 ×g for 5 min at 4°C. Twenty microliters of the lysate was mixed with 20 μl of 2× SDS sample buffer. The remaining lysate was adjusted to 250 μl with the lysis buffer and incubated for 2 h at 4°C after the addition of 20 μl of His-Select nickel affinity gel (Sigma) equilibrated 50% (vol/vol) with lysis buffer. The nickel beads that included SPP-wt or SPP-D219K were washed five times with 500 μl of lysis buffer by centrifugation at 5, 000 × *g* for 1 min at 4°C and then suspended in 40 μl of 1× SDS sample buffer. After being boiled at 60°C for 20 min, the supernatant was subjected to Western blotting to detect the coprecipitated core proteins.

Immunofluorescence microscopy. Huh7OK1 cells were incubated with fresh DMEM containing Bodipy 558/568 (2 μg/ml; Molecular Probes) for 1 h at 37°C to visualize lipid droplets (LDs). The cells were washed once with prewarmed DMEM and incubated for 30 min at 37°C. The treated cells were then fixed in 4% paraformaldehyde for 30 min at room temperature. After two washes with PBS, the cells were permeabilized with permeabilization buffer containing 0.1% saponin (eBioscience, San Diego, CA) for 30 min at 37°C and blocked with PBS containing 2% FBS (blocking buffer) for 30 min at room temperature. The cells were incubated with an appropriate antibody, as indicated in the figure legends. The cells were washed three times with PBS. The mounted cells were observed with a FluoView FV1000 laser scanning confocal microscope (Olympus, Tokyo, Japan). Nuclei were stained with 4′,6′-diamidino-2-phenylindole (DAPI).

Flotation assay. A flotation assay was carried out according to the method described previously (17). Briefly, 293FT cells expressing EHcVc or EHcVc-mt were cultured on a 10-cm dish. The transfected cells were washed once with cold PBS at 18 h posttransfection and harvested using a cell scraper. The cells were suspended in 1.2 ml of 25 mM Tris-HCl (pH 7.5) containing 150 mM NaCl, 5 mM EDTA, and protease inhibitor cocktail (Merck, Calbiochem) (TNE buffer) and were then homogenized by 10 passes through a 26-gauge needle. Each 0.6-ml aliquot of the homogenates was incubated for 30 min on ice with or without 1% Triton X-100 and was then mixed with 0.4 ml of OptiPrep (Axis-Shield, Oslo, Norway). An appropriate concentration of OptiPrep was adjusted with TNE buffer. This mixture was overlaid with 1.2 ml of 30% OptiPrep, 1.2 ml of 25% OptiPrep, and 0.8 ml of 5% OptiPrep, in that order, and was centrifuged at 42,000 rpm for 5 h at 4°C in an SW50.1 rotor (Beckman Coulter, Fullerton, CA). Each fraction, with a volume of 0.4 ml, was collected from the top of the centrifugation tube and was then precipitated by mixing with 4 volumes of cold acetone at −30°C. The resulting pellet was resolved in 50 μl of 1× sample buffer and then subjected to Western blot analysis using a mouse anti-FLAG antibody (Sigma), a rabbit anti-calreticulin antibody (Sigma), and a rabbit anti-caveolin-1 antibody (Sigma). The fractions containing calreticulin in the absence and presence of Triton X-100 were defined as the membrane and detergent-soluble membrane fractions, respectively. In the presence of the detergent, fractions 3 to 5, which contained caveolin-1 but only small amounts of calreticulin, were defined as the detergent-resistant membrane fractions.

Nucleotide sequence accession numbers. The whole sequence of the EHcV strain isolated from serum sample 3 was deposited in GenBank under accession number AB863589. The nucleotide sequences of the partial NS5B-coding regions and 3′ UTRs from samples 5 and 1 were registered as AB921150 and AB921151, respectively.

RESULTS

Detection of the EHcV genome and antibody to EHcV in sera of Japanese-born horses. To clarify whether NPHVs were distributed in Japan, we collected 31 horse serum samples and examined them in order to detect the EHcV genome and antibody to the core protein. We prepared total RNAs from horse sera and screened them using RT-PCR analyses with three sets of PCR primers (NPHV-F1/NPHV-R1, NPHV-F2/NPHV-R2, and NPHV-F3/NPHV-R3) that targeted the NS3-coding region that is relatively conserved among NPHVs. Total RNA prepared from conventional rabbit serum was used as a negative control. PCR products with the expected sizes were found in horse serum samples 1, 3, 25, 26, 27, and 29 to 31 using NPHV-F1/NPHV-R1, in horse serum samples 3 and 5 using NPHV-F2/R2, and in horse serum samples 1, 3, 5, 20, and 25 to 31 using NPHV-F3/R3 (Fig. 1A). The EHcV genome was detected in 11 of 31 (35%) serum samples by RT-PCR (Fig. 1A and B). Copy numbers of the EHcV genome in horse sera varied from 10^4 to 10^9 copies per ml of sera (Fig. 1B). Although a PCR product was slightly amplified from serum sample 19 by PCR using the primer pair NPHV-F1/R1, the copy number of the virus genome in serum sample 19 was estimated to be low, at a level similar to that of the negative control. Thus, we could not determine whether serum sample 19 included a viral genome. We then immunologically surveyed horse sera by Western blotting. Western blotting analyses using horse sera to detect antibodies to the EHcV core protein (Fig. 2) showed that the sera of samples 1, 2, 3, 5, 14, 20, and 25 were immunoreactive to the EHcV core protein (7 positive serum samples of a total of 31 samples; 22.6%). The sera of samples 1, 3, 5, and 20 were PCR positive and seropositive. Serum samples 2 and 14 were PCR negative and seropositive, whereas samples 26 to 31 were PCR positive and seronegative. These results suggest that EHcV has infected Japanese-born domestic horses.

Genetic analysis of EHcV. PCR products corresponding to the 5′ UTR and the open reading frame were segmentally amplified from serum sample 3 by 5′ RACE and RT-PCR, respectively. In the present study, we successfully determined the 3′-terminal sequence downstream of a stop codon using the 3′-RACE method with poly(U) polymerase. We determined the nucleotide sequence of the putative full genome, which was designated JPN3/JAPAN/2013 (GenBank accession number AB863589). The full-length genome of strain JPN3/JAPAN/2013 is composed of 9,355 nucleotides, consisting of the 5′ UTR with a nucleotide length of 389, the 3′ UTR with a nucleotide length of 134, and an open

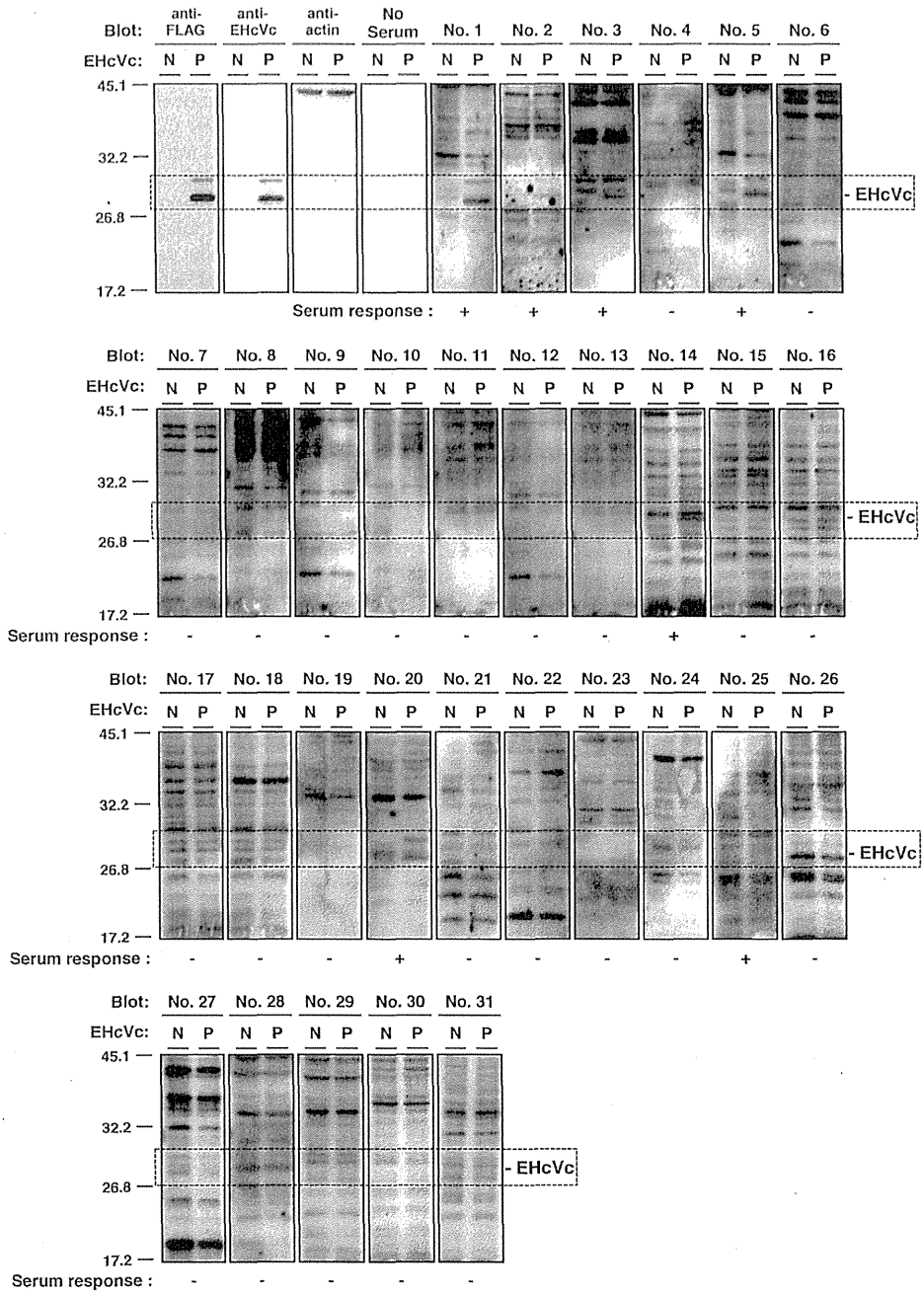

FIG 2 Serological screening of Japanese-born domestic horses. Lysates of 293FT cells transfected with an empty plasmid (a negative reference, N) or the plasmid encoding EHcVc (a positive reference, P) were subjected to Western blotting using serum from each horse. The serum response "+" indicates that the protein band with the same molecular size as the EHcV core protein was specifically detected in the "P" lane, but not in the "N" lane, while the serum response "–" indicates that the protein band with the same molecular size as the EHcV core protein was detected in neither the "P" lane nor the "N" lane. Both antibodies to the FLAG tag and to the EHcV core protein were used as serum positive controls, while protein amounts were standardized with blotting using the antibody to beta-actin. "No serum" indicates the membrane was incubated without primary antibodies but with HRP-conjugated anti-horse IgG antibodies as a background of the secondary antibody.

reading frame with a nucleotide length of 8,832. The open reading frame encodes 2,943 amino acids. Table 2 summarizes the amino acid homology of the JPN3/JAPAN/2013 polyprotein with the polyproteins of the other EHcV strains. The polyprotein of JPN3/JAPAN/2013 shared more than 94% homology with the other EHcV polyproteins and exhibited the highest homology, 97.8%, with NPHV-H10-094 (GenBank accession number JQ434007), which was isolated from a horse in the United States (8). The NS3- and NS5B-coding regions of the EHcV strains were phylogenetically analyzed by the neighbor-joining method. The phylogenetic